JOURNAL OF GUIDANCE, CONTROL, AND DYNAMICS
Vol. 32, No. 6, November–December 2009

State Transition Matrix Approximation Using a Generalized Averaging Method

Yuichi Tsuda*
Japan Aerospace Exploration Agency, Kanagawa 229-8510, Japan
and
Daniel J. Scheeres†
University of Colorado at Boulder, Boulder, Colorado 80309

DOI: 10.2514/1.44142

This paper presents a method for approximating the state transition matrix for orbits around a primary body and subject to arbitrary perturbations. A generalized averaging method is employed to isolate the high- and low-frequency regions of the perturbation terms and to construct a functional form of the approximate state transition matrix composed only of elementary analytic functions. The resulting state transition matrix is expressed with a small number of constant parameter matrices and osculating orbit parameters at an initial epoch and is valid for tens of orbital revolutions without having to update the parameters. Numerical simulations show that this method is valid for arbitrary-eccentricity orbits with semimajor axes ranging from low Earth orbit up to around 10 Earth radii when applied to Earth orbits. This method has been developed for implementation onboard spacecraft for high-accuracy formation-flying missions. Furthermore, it is shown that the symplectic property, which is a fundamental mathematical structure of Hamiltonian systems, can be incorporated into the method. This not only reduces the number of parameters required for approximations, but also preserves the physically true structure of the state transition matrix and provides some important properties that are useful for practical onboard computation.

I. Introduction

A METHOD for approximating state transition matrices for fully perturbed orbital dynamics is described in this paper. The generalized averaging method for linear differential equations with almost-periodic coefficients [1] is applied to derive a simple form for fully perturbed state transition matrices, composed only of elementary analytic functions and a small number of parameter matrices. The primary advantage of this method is that it can provide a simple mathematical form of a fully perturbed state transition matrix that is especially suited to use on onboard systems.

There are numerous studies on state transition matrices for orbital dynamics. The earliest studies on this problem were performed by Hill [2] and Clohessy and Wiltshire [3], who derived the linearized behavior of neighboring orbits of a circular reference orbit assuming two-body dynamics. Lawden [4] developed linearized orbital motion around an eccentric reference orbit, which also assumes two-body dynamics, and its solution form was improved by Carter and Humi [5] and Carter [6].

Most recent developments in theories for the orbital state transition matrix stem from a growing demand for and development of formation-flight technologies. It has been found that even for proximity relative orbital motion, it may be insufficient to only consider the linearized dynamics of Keplerian motions to obtain even moderately accurate relative orbital motions.

Research to overcome this has mainly occurred in three ways. The first direction is to add realistic perturbation effects. For example, the linearized effect of the J2 term can be analytically derived and included into the state transition matrix around circular or eccentric orbits [7–11]. The second direction of study is to take into account not only linearized behavior, but also nonlinear effects. Alfriend et al. [12] gave a second-order relative motion based on Keplerian elements representations. Vaddi et al. [13] presented a state transition matrix that includes the effects of eccentricity, gravitational perturbations and nonlinearities. Melton [14] presented a state transition matrix approach incorporating higher-order eccentricity terms. Park and Scheeres [15] proposed a higher-order Taylor series expansion approach to apply to general (perturbed) trajectories. There are also geometric approaches [16,17] that directly consider the form of solutions for relative orbital motions, rather than linearizing the orbital equations of motion. The third direction is to capture the precise mathematical structure of relative orbital motions. Palmer and Imre [18] derived second-order relative Keplerian motions that precisely conserve the relative Hamiltonian and relative angular momentum. Imre and Palmer [19] presented an integration method of relative orbital motions that exactly conserves the symplectic structure of Hamiltonian system. Tsuda and Scheeres [20] derived a generalized method of solving the symplectic state transition matrix and applied it to fully perturbed relative orbital motions around eccentric Earth orbits and Halo orbits.

On the other hand, many formation-flight missions are proposed or planned with demanding requirements [21]. It is natural to think that larger numbers of satellites with more accurate formation-keeping and control capabilities will be required in the future. For highly autonomous formation control, a precise model of the relative orbital motion must be implemented onboard the spacecraft. This situation is highlighted when a large number of spacecraft are involved, or only infrequent ground support is expected. Thus, for highly accurate autonomous formation flying, not only precise but also simple mathematical representations of relative orbital motions are important.

The aim of this paper is to provide a simple mathematical form for the state transition matrix under a fully perturbed environment. Distinct from the past studies introduced earlier, this method provides a simple functional form of the state transition matrix and provides a method of parameter matching to model state transition matrices for precise relative orbital motions incorporating a variety of practical perturbation sources, such as geopotential perturbations and third-body perturbations. Past studies mainly consider differential geopotential effects as a source of perturbation, but third-body

Received 4 March 2009; revision received 13 June 2009; accepted for publication 13 June 2009.

*Assistant Professor, Institute of Space and Astronautical Science, Department of Space Systems and Astronautics, 3-1-1, Yoshinodai, Sagamihara. Member AIAA.

†A. Richard Seebass Endowed Chair Professor, 429 UCB. Member AIAA.

perturbations and other perturbation sources may become important for formation flight in high-eccentricity, large-semimajor-axis orbit; hence, they are also considered in this study. Sengupta et al. [22] provided an averaged solution for the eccentric relative motions incorporating J2, and the parameters appearing in the formulation are given analytically. In contrast with that, the approximation method discussed in this paper provides the solution form of the state transition matrix with arbitrary perturbations, though the parameters appearing in the solution form must be determined numerically by curve-fitting to a numerically integrated trajectory. The resulting mathematical form of the state transition matrix is simple enough to implement on a spacecraft's onboard computer without demanding high performance. Because this method provides a simple way of interpolating accurate state transition matrices, which usually requires heavy computational loads and excessive times, this method is also useful for offline analysis when fast and iterative computations of accurate state transition matrices are required.

This paper is composed as follows. In Sec. II, some basic derivations of relative orbital dynamics are given to be used in the following sections. A group of almost-periodic functions, which we assume to be the general form of the perturbation forces, is also introduced with some useful formulas. In Sec. III, a generalized averaging method is applied to the relative orbital dynamics, and the functional form of the perturbed state transition matrix is derived. The parameter-matching process and its optimal strategy are also described. Section IV provides numerical validations for the derived approximation method under geopotential and third-body perturbations with various orders of approximation. The applicability limit of this method is also assessed in this section. Section V incorporates the symplectic structure into this approximation method. Because nondissipative relative orbital motion forms a Hamiltonian system, it must have a symplectic structure by nature. It is shown in this section that by taking into account the symplecticity, higher accuracy for the geometrical structure of the state transition matrix is obtained with fewer parameters required. Section VI is the conclusion of this paper. In Appendices A and B, the solution of two-body relative orbital motion and the generalized averaging method for linear differential equations with almost-periodic coefficients, which are used throughout this paper, are described for reference.

II. Relative Orbital Dynamics as an Almost-Periodic Function

In this section, we will provide linearized equations of motion for relative orbital dynamics. Although the derivation is according to a standard procedure of linearization, a fully perturbed relative orbit is linearized about a perturbed reference orbit and is expressed only using osculating orbit information at an initial epoch. We chose the true anomaly, instead of the time, for the dependent variable. The true-anomaly representation enables us to deal with orbital dynamics always as a function of a 2π-periodic dependent variable regardless of the presence of perturbations and thus eliminates the secular effect due to the change in orbital period itself.

A. Perturbed Orbit Linearized About a Keplerian Orbit

Orbital motions under two-body (Keplerian) dynamics and perturbation force are expressed, respectively, as

$$\ddot{\mathbf{r}}_N = -\frac{\mu}{r_N^3}\mathbf{r}_N \tag{1}$$

$$\ddot{\mathbf{r}}_O = -\frac{\mu}{r_O^3}\mathbf{r}_O + \varepsilon\mathbf{f}(\mathbf{r}_O, t) \tag{2}$$

where $\mathbf{r}_N$ and $\mathbf{r}_O$ are position vectors subject to the gravity of the primary body with the gravity constant μ, without and with perturbation force, respectively, and $\varepsilon\mathbf{f}$ is an arbitrary perturbation force with ε assumed to be small. The subtraction of Eq. (1) from Eq. (2) gives, to the first order,

$$\begin{aligned}\ddot{\mathbf{r}}_O - \ddot{\mathbf{r}}_N \triangleq \delta\ddot{\mathbf{r}}_{ON} &= -\left(\frac{\mu}{r_O^3}\mathbf{r}_O - \frac{\mu}{r_N^3}\mathbf{r}_N\right) + \varepsilon\mathbf{f}(\mathbf{r}_O, t)\\ &= \left\{-\frac{\mu}{r_N^3}\left(\mathbf{1}_{3\times3} - \frac{\mathbf{r}_N\mathbf{r}_N^T}{r_N^2}\right) + \varepsilon\left.\frac{\partial\mathbf{f}(\mathbf{r}, t)}{\partial\mathbf{r}}\right|_{\mathbf{r}=\mathbf{r}_N}\right\}\delta\mathbf{r}_{ON}\\ &\quad + \varepsilon\mathbf{f}(\mathbf{r}_N, t) + O(\varepsilon^2)\end{aligned} \tag{3}$$

where $\mathbf{1}_{n\times n}$ denote the $n \times n$ identity matrix. The final transformation uses a linearization around the Keplerian orbit. If we rewrite Eq. (3) in the form of matrix differential equation, it becomes

$$\delta\dot{\mathbf{x}}_{ON} = \begin{bmatrix}\mathbf{0}_{3\times3} & \mathbf{1}_{3\times3}\\ \mathbf{G}_N(t) + \delta\mathbf{G}_{ON}(t) & \mathbf{0}_{3\times3}\end{bmatrix}\delta\mathbf{x}_{ON} + \varepsilon\begin{bmatrix}\mathbf{0}_{3\times1}\\ \mathbf{f}(\mathbf{r}_N, t)\end{bmatrix} \tag{4}$$

where we define

$$\delta\mathbf{x}_{ON} = \begin{bmatrix}\delta\mathbf{r}_{ON}\\ \delta\dot{\mathbf{r}}_{ON}\end{bmatrix}, \qquad \mathbf{G}_N(t) = -\frac{\mu}{r_N^3}\left(\mathbf{1} - \frac{\mathbf{r}_N\mathbf{r}_N^T}{r_N^2}\right)$$
$$\delta\mathbf{G}_{ON}(t) = \varepsilon\left.\frac{\partial\mathbf{f}(\mathbf{r}, t)}{\partial\mathbf{r}}\right|_{\mathbf{r}=\mathbf{r}_N} \tag{5}$$

and $\mathbf{0}_{n\times m}$ is the $n \times m$ null matrix.

Now let us introduce the conversion matrix from the time-domain expression to the true-anomaly-domain expression, such that

$$\delta\mathbf{x}_\theta(\theta) = \begin{bmatrix}\delta\mathbf{r}(\theta)\\ \delta\mathbf{r}'(\theta)\end{bmatrix} = \mathbf{T}\delta\mathbf{x}(t) = \begin{bmatrix}\mathbf{1} & \mathbf{0}\\ \mathbf{0} & \frac{1}{\dot\theta}\mathbf{1}\end{bmatrix}\begin{bmatrix}\delta\mathbf{r}\\ \delta\dot{\mathbf{r}}\end{bmatrix}$$
$$\dot\theta = \frac{\omega_N(1 - e\cos\theta)^2}{(1 - e^2)^{3/2}} \tag{6}$$

where θ is the true anomaly, $\delta\mathbf{x}_\theta(\theta)$ is the state vector expressed in θ domain, $(\bullet)' \triangleq (\mathrm{d}/\mathrm{d}\theta)(\bullet)$, and ω_N and e are the natural frequency and the eccentricity of the orbit, respectively.

By applying Eq. (6) to Eq. (4), we obtain the linearized equation expressed with the dependent variable θ, which is of the form

$$\delta\mathbf{x}'_{\theta ON} = \{\mathbf{A}_{\theta N}(\theta) + \delta\mathbf{A}_{\theta ON}(\theta)\}\delta\mathbf{x}_{\theta ON} + \varepsilon\mathbf{b}_\theta(\theta) \tag{7}$$

where we denote

$$\mathbf{A}_{\theta N}(\theta) = \frac{1}{\dot\theta}\{\dot{\mathbf{T}}(\theta)\mathbf{T}(\theta)^{-1} + \mathbf{T}(\theta)\mathbf{A}_N(\theta)\mathbf{T}(\theta)^{-1}\}$$
$$\mathbf{A}_N(\theta) = \begin{bmatrix}\mathbf{0}_{3\times3} & \mathbf{1}_{3\times3}\\ \mathbf{G}_N(\theta) & \mathbf{0}_{3\times3}\end{bmatrix}, \qquad \delta\mathbf{A}_{\theta ON}(\theta) = \frac{1}{\dot\theta}\begin{bmatrix}\mathbf{0} & \mathbf{0}\\ \delta\mathbf{G}_{ON}(\theta) & \mathbf{0}\end{bmatrix}$$
$$\mathbf{b}_\theta(\theta) = \varepsilon\frac{1}{\dot\theta}\begin{bmatrix}\mathbf{0}\\ \mathbf{f}(\mathbf{r}_N, \theta)\end{bmatrix} \tag{8}$$

Note that because $\mathbf{T}(\theta)$ and $\mathbf{A}_N(\theta)$ are periodic functions with the orbital period of the Keplerian dynamics, $\mathbf{A}_{\theta N}(\theta)$ is a periodic function of θ with the period 2π.

Furthermore, we know that the nonperturbed linearized equations of motion, which are obtained by applying $\varepsilon = 0$ to Eq. (7), can be solved analytically and can be written in the following general form:

$$\delta\mathbf{x}_{\theta ON}(\theta_1) = \mathbf{\Phi}_{\theta N}(\theta_1, \theta_0)\delta\mathbf{x}_{\theta ON}(\theta_0) \quad \text{if } \varepsilon = 0 \tag{9}$$

where $\mathbf{\Phi}_{\theta N}$ is the state transition matrix of Keplerian dynamics expressed within the θ domain. It takes the form

$$\mathbf{\Phi}_{\theta N}(\theta, 0) = \mathbf{1}_{6\times6} + \frac{\theta}{2\pi}\mathbf{W}_0 + \sum_{m\geq1}\{\mathbf{\Phi}_{\theta Ncm}\cos m\theta + \mathbf{\Phi}_{\theta Nsm}\sin m\theta\} \tag{10}$$

where $\mathbf{W}_0$, $\mathbf{\Phi}_{\theta Ncm}$, and $\mathbf{\Phi}_{\theta Nsm}$ are all constant matrices. See Appendix A for the full detail of Eq. (10).

B. Perturbed Relative Orbital Motion of Two Spacecraft

This subsection considers the motion of a follower satellite, linearized around the orbit of the leader satellite. We consider the perturbed orbits for the leader and follower satellites and attempt to express the relative motion using only information from a Keplerian reference orbit.

If the leader's orbit is given by Eq. (2) and the follower's is given by

$$\ddot{\mathbf{r}}_P = -\frac{\mu}{r_P^3}\mathbf{r}_P + \varepsilon\mathbf{f}(\mathbf{r}_P, t) \tag{11}$$

where $\mathbf{r}_P$ is the position of the follower, the relative orbit between the leader and the follower can be written as

$$\begin{aligned}\ddot{\mathbf{r}}_P - \ddot{\mathbf{r}}_O \triangleq \delta\ddot{\mathbf{r}}_{PO} &= -\left(\frac{\mu}{r_P^3}\mathbf{r}_P - \frac{\mu}{r_O^3}\mathbf{r}_O\right) + \varepsilon(\mathbf{f}(\mathbf{r}_P, t) - \mathbf{f}(\mathbf{r}_O, t)) \\ &= \left\{-\frac{\mu}{r_O^3}\left(\mathbf{1}_{3\times3} - \frac{\mathbf{r}_O\mathbf{r}_O^T}{r_O^2}\right) + \varepsilon\frac{\partial\mathbf{f}^I(\mathbf{r}, t)}{\partial\mathbf{r}}\bigg|_{\mathbf{r}=\mathbf{r}_O}\right\}\delta\mathbf{r}_{PO} + O(\varepsilon^2)\end{aligned} \tag{12}$$

Since $\mathbf{r}_O = \mathbf{r}_N + \delta\mathbf{r}_{ON}$, Eq. (12) is further transformed to

$$\begin{aligned}\delta\ddot{\mathbf{r}}_{PO} \approx \Bigg[&-\frac{\mu}{r_N^3}\left(\mathbf{1}_{3\times3} - \frac{\mathbf{r}_N\mathbf{r}_N^T}{r_N^2}\right) + \frac{3\mu}{r_N^3}\left\{\left(\mathbf{1}_{3\times3} - \frac{5\mathbf{r}_N\mathbf{r}_N^T}{r_N^2}\right)\frac{\delta r_{ON}}{r_N}\right. \\ &\left. + \frac{\delta\mathbf{r}_{ON}\mathbf{r}_N^T + \mathbf{r}_N\delta\mathbf{r}_{ON}^T}{r_N^2}\right\} + \varepsilon\frac{\partial\mathbf{f}(\mathbf{r}, \theta)}{\partial\mathbf{r}}\bigg|_{\mathbf{r}=\mathbf{r}_N}\Bigg]\delta\mathbf{r}_{PO}\end{aligned} \tag{13}$$

where $\delta\mathbf{r}_{ON}$ and ε are treated to be very small and are taken up to first order. Equation (13) is transformed to the form of a matrix differential equation as

$$\delta\dot{\mathbf{x}}_{PO} = \begin{bmatrix}\mathbf{0}_{3\times3} & \mathbf{1}_{3\times3} \\ \mathbf{G}_N(t) + \delta\mathbf{G}_{PO}(t) & \mathbf{0}_{3\times3}\end{bmatrix}\delta\mathbf{x}_{PO} \tag{14}$$

with

$$\delta\mathbf{x}_{PO} = \begin{bmatrix}\delta\mathbf{r}_{PO} \\ \delta\dot{\mathbf{r}}_{PO}\end{bmatrix}$$

$$\begin{aligned}\delta\mathbf{G}_{PO}(t) = &\frac{3\mu}{r_N^3}\left\{\left(\mathbf{1}_{3\times3} - \frac{5\mathbf{r}_N\mathbf{r}_N^T}{r_N^2}\right)\frac{\delta r_{ON}}{r_N} + \frac{\delta\mathbf{r}_{ON}\mathbf{r}_N^T + \mathbf{r}_N\delta\mathbf{r}_{ON}^T}{r_N^2}\right\} \\ &+ \varepsilon\frac{\partial\mathbf{f}(\mathbf{r}, \theta)}{\partial\mathbf{r}}\bigg|_{\mathbf{r}=\mathbf{r}_N}\end{aligned} \tag{15}$$

and $\mathbf{G}_N(t)$ is given in Eq. (5).

In the same way as we did with Eqs. (4–8), we can transform Eq. (14) to the equation expressed with the dependent variable θ. It takes the form

$$\delta\mathbf{x}'_{\theta PO} = \{\mathbf{A}_{\theta N}(\theta) + \delta\mathbf{A}_{\theta PO}(\theta)\}\delta\mathbf{x}_{\theta PO} \tag{16}$$

where

$$\delta\mathbf{A}_{\theta PO}(\theta) = \frac{1}{\dot{\theta}}\begin{bmatrix}\mathbf{0} & \mathbf{0} \\ \delta\mathbf{G}_{PO}(\theta) & \mathbf{0}\end{bmatrix} \tag{17}$$

and $\mathbf{A}_{\theta N}(\theta)$ is already defined in Eq. (8).

It can be seen from Eq. (16) that, as we saw in Eq. (8), $\mathbf{A}_{\theta N}(\theta)$ is a periodic function of θ with period 2π. We can also see that $\delta\mathbf{A}_{\theta PO}(\theta)$ is a function of $\mathbf{P}$, $\mathbf{r}_N$, $\delta\mathbf{r}_{ON}$, and $\varepsilon\mathbf{f}$, and in these, only $\delta\mathbf{r}_{ON}$ and $\varepsilon\mathbf{f}$ are the variables that are not 2π-periodic.

C. Almost-Periodic Function Group and Its Characteristics

Though this subsection is rather independent, we introduce a group of almost-periodic functions of a special form to prepare for discussions in the following sections.

Let $\mathfrak{M}$ denote the group of almost-periodic functions defined as

$$\mathfrak{M} \triangleq \left\{f(\theta)|f(\theta) \in \mathfrak{M}, f(\theta) = \sum_{-\infty<n<\infty}\sum_{-\infty<m<\infty} f_{mn}e^{in\theta}e^{i\varepsilon\hat{\omega}_m\theta}\right\} \tag{18}$$

where n and m are integers, and $\varepsilon\hat{\omega}_m$ is a normalized angular velocity and is slower than the unit frequency ($\varepsilon\hat{\omega}_m < 1$). Here, f and f_{mn} can be scalars or elements of a vector or matrix. Equation (18) states that $f(\theta)$ in $\mathfrak{M}$ consists of the frequency that is an integer multiple of 2π, modulated by slower frequencies represented by $\varepsilon\hat{\omega}_m$. If $f(\theta)$ is a real function, then we can impose

$$\varepsilon\hat{\omega}_m = -\varepsilon\hat{\omega}_{(-m)} \tag{19}$$

without losing generality.

Then let us introduce the following two operators:

$$L_{\hat{\omega}_c}[e^{i\hat{\omega}\theta}] = \begin{cases}e^{i\hat{\omega}\theta} & (\hat{\omega} < \hat{\omega}_c) \\ 0 & (\hat{\omega} \geq \hat{\omega}_c)\end{cases} \tag{20a}$$

$$H_{\hat{\omega}_c}[e^{i\hat{\omega}\theta}] = \begin{cases}\frac{1}{i\hat{\omega}}e^{i\hat{\omega}\theta} & (\hat{\omega} \geq \hat{\omega}_c) \\ 0 & (\hat{\omega} < \hat{\omega}_c)\end{cases} \tag{20b}$$

These are called the averaging operator and integration operator, respectively. These operators extract the low- and high-frequency parts from the original functions, respectively.

For a general function in $\mathfrak{M}$, when taking $\hat{\omega}_c = \min|1 + \varepsilon\hat{\omega}_m|$, the operator's effect is as follows:

$$L_{\min|1+\varepsilon\hat{\omega}_m|}[f(\theta)] = \sum_{-\infty<m<\infty} f_{m0}e^{i\varepsilon\hat{\omega}_m\theta} \tag{21}$$

$$\begin{aligned}&H_{\min|1+\varepsilon\hat{\omega}_m|}[f(\theta)] \\ &\quad= \sum_{\substack{-\infty<n<\infty \\ n\neq0}}\sum_m \frac{1}{i(n + \varepsilon\hat{\omega}_m)}f_{mn}e^{i(n+\varepsilon\hat{\omega}_m)\theta}\end{aligned} \tag{22}$$

where we assume

$$\max|\varepsilon\hat{\omega}_m| < \min|1 + \varepsilon\hat{\omega}_m| \tag{23}$$

Note that from the form of Eq. (21), we see that

$$L_{\min|1+\varepsilon\hat{\omega}_m|}[f(\theta)] = f(2\pi l)|_{l=\theta/2\pi} + c^* \tag{24}$$

where c^* is a certain constant. Equation (24) provides a way to extract the low-frequency part. Although this does not give us a concrete expression for c^*, we get from Eq. (24) the low-frequency component of the spectrum of $f(\theta)$.

For example, if we take the state transition matrix for Keplerian dynamics of the form in Eq. (10), it is found to be a member of $\mathfrak{M}$. Indeed, Eq. (10) is obtained by substituting in Eq. (18) such that

$$f_{nm}e^{i\varepsilon\hat{\omega}_m\theta} \mapsto \begin{cases}\mathbf{1} & m = 0, n = 0 \\ \frac{\theta}{2\pi}\mathbf{W}_0 & m \neq 1, n = 0 \\ \mathbf{C}_n\cos n\theta + \mathbf{S}_n\sin n\theta & m = 0, n \neq 0 \\ \mathbf{0} & \text{others}\end{cases} \tag{25}$$

Applying the averaging and integrating operators for $\hat{\omega}_c = 1$ gives

$$L_1[\mathbf{\Phi}(\theta, 0)] = \mathbf{1} + \frac{\theta}{2\pi}\mathbf{W}_0 \tag{26a}$$

$$H_1[\mathbf{\Phi}(\theta, 0)] = \sum_n \frac{1}{n}[\mathbf{C}_n\cos n\theta + \mathbf{S}_n\sin n\theta] \tag{26b}$$

On the other hand, applying Eq. (24) to Eq. (10) provides, with a certain constant matrix $\mathbf{C}^*$,

$$\mathbf{\Phi}(2\pi l, 0)|_{l=2\pi/\theta} + \mathbf{C}^* = \mathbf{1} + \frac{\theta}{2\pi}\mathbf{W}_0 + \sum_n \mathbf{C}_n + \mathbf{C}^* \tag{27}$$

which is found to be equivalent to Eq. (26a) when we set

$$\mathbf{C}^* = -\sum_n \mathbf{C}_n$$

The general perturbation force acting on the object relative to a Keplerian reference orbit can be written as a function of a two-body orbit position vector $\mathbf{r}_0(\theta)$, which is 2π-periodic, modulated by the frequency of perturbation sources, represented by $\varepsilon\hat{\omega}_{pm}$. For example, if we consider a third-body perturbation, the perturbation force is a function of $\mathbf{r}_0(\theta)$ and the position of the third-body $\mathbf{R}(\varepsilon\hat{\omega}_p\theta)$, which is a $2\pi/\hat{\omega}_p$-periodic vector. Hence, the perturbation force of this type satisfies $\mathbf{f}(\mathbf{r}_0(\theta), \mathbf{R}(\varepsilon\hat{\omega}_p\theta)) \in \mathfrak{M}$. Thus,

$$\mathbf{f}(\mathbf{r}_0(\theta), \mathbf{R}(\varepsilon\hat{\omega}_p\theta)) = \sum_{-\infty<n<\infty} \sum_{-\infty<m<\infty} \mathbf{f}_{mn} e^{in\theta} e^{i\varepsilon m\hat{\omega}_p\theta} \tag{28}$$

Then from Eq. (24), we get

$$L_{\min|1+\varepsilon m\hat{\omega}_p|}[\mathbf{f}(\mathbf{r}_0(0), \mathbf{R}(\varepsilon\hat{\omega}_p\theta))] = \sum_{-\infty<m<\infty} \mathbf{f}_{m0} e^{i\varepsilon m\hat{\omega}_p\theta} + \mathbf{c}^* \tag{29}$$

where $\mathbf{c}^*$ is a certain constant, and we assume

$$\max|\varepsilon m\hat{\omega}_p| < \min|1 + \varepsilon m\hat{\omega}_p| \tag{30}$$

As m generally takes integer values ranging from negative infinity to positive infinity, it must be truncated to a reasonable order to satisfy Eq. (28). For example, a truncated function of Eq. (28) (in terms of m) can be written as

$$\tilde{\mathbf{f}}(\mathbf{r}_0(\theta), \mathbf{R}(\varepsilon\hat{\omega}_p\theta)) \triangleq \sum_{-\infty<n<\infty} \sum_{-m_t<m<m_t} \mathbf{f}_{mn} e^{in\theta} e^{i\varepsilon m\hat{\omega}_p\theta} \tag{31}$$

and the first-order accuracy is satisfied when

$$\|\mathbf{f}(\mathbf{r}_0(\theta), \mathbf{R}(\varepsilon\hat{\omega}_p\theta)) - \tilde{\mathbf{f}}(\mathbf{r}_0(\theta), \mathbf{R}(\varepsilon\hat{\omega}_p\theta))\| < O(\varepsilon) \quad \text{and} \quad \varepsilon m_t\hat{\omega}_p < 1 - \varepsilon m_t\hat{\omega}_p \tag{32}$$

for appropriate $m_t > 0$. Note that if we consider $\mathbf{R}(\varepsilon\hat{\omega}_p\theta)$ not of the third body, but from the other perturbation sources, it is still valid as long as $\varepsilon\hat{\omega}_p$ can be assumed to be sufficiently small.

In the end of this subsection, let us derive formulas that will be used in the following section. For $f(\theta)$ and $g(\theta)$ in $\mathfrak{M}$, we can calculate

$$f(\theta) \bullet \{H_{\min|1+\varepsilon\hat{\omega}_{fm}+\varepsilon\hat{\omega}_{gl}|}[g(\theta)]\} = \sum_{-\infty<n<\infty} \sum_m \sum_{\substack{-\infty<k<\infty \\ k\neq 0}} \sum_l f_{mn} g_{lk} e^{i(n+k+\varepsilon\hat{\omega}_{fm}+\varepsilon\hat{\omega}_{gl})\theta} \tag{33}$$

$$\{L_{\min|1+\varepsilon\hat{\omega}_{fm}+\varepsilon\hat{\omega}_{gl}|}[f(\theta)]\} \bullet \{H_{\min|1+\varepsilon\hat{\omega}_{fm}+\varepsilon\hat{\omega}_{gl}|}[g(\theta)]\} = \sum_m \sum_{\substack{-\infty<k<\infty \\ k\neq 0}} \sum_l f_{m0} g_{lk} e^{i(k+\varepsilon\hat{\omega}_{fm}+\varepsilon\hat{\omega}_{gl})\theta} \tag{34}$$

These suggest that

$$L_{\hat{\omega}_c}[f \bullet H_{\hat{\omega}_c}[g]] = L_{\hat{\omega}_c}[L_{\hat{\omega}_c}[f] \bullet H_{\hat{\omega}_c}[g]] = 0 \quad \text{if } \hat{\omega}_c = \min|1 + \varepsilon\hat{\omega}_{fm} + \varepsilon\hat{\omega}_{gl}| \tag{35}$$

III. Derivation of the State Transition Matrix Approximation

Based on the discussions in the previous section, this section provides an analytical derivation of the approximate state transition matrix. We apply the generalized averaging method for linear differential equations with almost-periodic coefficients to our system and derive the averaged state transition matrix that eliminates the frequencies equal to or higher than the orbital frequency. To apply the generalized averaging method, we impose the following assumptions throughout this paper.

1) The perturbation effect we take into account is sufficiently slow and small. The perturbation frequency is of the order of ε when compared with the orbital frequency, and its magnitude is also of the order of ε when compared with the gravity force of the primary planetary body.

2) The effect of perturbations with frequencies higher than or equal to the orbital frequency is to be treated as additional terms to the averaged solution.

3) Only up to first-order behavior (i.e., of the order of ε) is taken into account.

The first assumption enables us to take into account perturbations due to third bodies and solar radiation pressure. The second assumption is for nonslow perturbations such as J2 and higher-gravitational effects and atmospheric drag. The third assumption simplifies the derivation process at the cost of accuracy, which will be evaluated in the later sections.

A. Averaged Motion of the Perturbed Reference Orbit

Consider the averaged solution for the differential equation with initial conditions given in Eq. (7). Again, that is

$$\delta\mathbf{x}'_{\theta ON} = \{\mathbf{A}_{\theta N}(\theta) + \delta\mathbf{A}_{\theta ON}(\theta)\}\delta\mathbf{x}_{\theta ON} + \varepsilon\mathbf{b}_\theta(\theta), \quad \delta\mathbf{x}_{\theta ON}(0) = \mathbf{0} \tag{36}$$

This imposes that the perturbed reference orbit coincides with the Keplerian orbit at $\theta = 0$. In another words, we use the osculating orbit parameters of $\theta = 0$.

To apply the generalized averaging method, we first need to transform Eq. (36) to a homogeneous differential equation with small coefficients. For this purpose, first, let us define the new state vector:

$$\delta\boldsymbol{\xi}_{ON}(\theta) = \{\delta\xi_i(\theta)\} = \begin{bmatrix} \delta\mathbf{x}_{\theta ON}(\theta) \\ \delta\xi_7(\theta) \end{bmatrix} \tag{37}$$

This is defined by adding the seventh state to the original state vector $\delta\mathbf{x}_{\theta ON}$. With this state vector, we can rewrite Eq. (36) as

$$\delta\boldsymbol{\xi}'_{ON}(\theta) = \begin{bmatrix} \mathbf{A}_{\theta N}(\theta) + \delta\mathbf{A}_{\theta ON}(\theta) & \varepsilon\mathbf{b}_\theta(\theta) \\ \mathbf{0}_{1\times 6} & 0 \end{bmatrix}\delta\boldsymbol{\xi}_{ON}(\theta), \quad \delta\boldsymbol{\xi}_{ON}(0) = \begin{bmatrix} \mathbf{0}_{6\times 1} \\ 1 \end{bmatrix} \tag{38}$$

which has now become a homogeneous differential equation. To transform further to a differential equation with sufficiently small coefficients, let us introduce the transformation from $\delta\boldsymbol{\xi}_{ON}$ to $\delta\boldsymbol{\zeta}_{ON}$ using

$$\delta\boldsymbol{\xi}_{ON}(\theta) = \begin{bmatrix} \mathbf{\Phi}_{\theta N}(\theta, 0) & \mathbf{0}_{6\times 1} \\ \mathbf{0}_{1\times 6} & 1 \end{bmatrix}\delta\boldsymbol{\zeta}_{ON}(\theta) \triangleq \mathbf{\Xi}(\theta)\delta\boldsymbol{\zeta}_{ON}(\theta) \tag{39}$$

where $\delta\boldsymbol{\zeta}_{ON}(\theta)$ can be interpreted as a virtual initial state at $\theta = 0$ calculated backward from the current state vector, when assuming that the state vector is subject only to the Keplerian dynamics. Because, in reality, the state vector is affected by perturbations, $\delta\boldsymbol{\zeta}_{ON}$ becomes a function of θ.

Using Eq. (38), Eq. (39) can be transformed as

$$\delta\boldsymbol{\zeta}'_{ON}(\theta) = \mathbf{\Xi}^{-1}(\theta)\begin{bmatrix} \delta\mathbf{A}_{\theta ON}(\theta) & \varepsilon\mathbf{b}_\theta(\theta) \\ \mathbf{0}_{1\times 6} & 0 \end{bmatrix}\mathbf{\Xi}(\theta)\delta\boldsymbol{\zeta}_{ON}(\theta), \quad \delta\boldsymbol{\zeta}_{ON}(0) = \begin{bmatrix} \mathbf{0}_{6\times 1} \\ 1 \end{bmatrix} \tag{40}$$

As we know from Eqs. (5) and (8) that both $\delta\mathbf{A}_{\theta ON}(\theta)$ and $\varepsilon\mathbf{b}_\theta(\theta)$ are of the order of ε, Eq. (40) can be said to be a homogeneous differential equation with a small coefficient of the order ε.

Now let us apply the generalized averaging method to Eq. (40), which is of the type

$$\delta\boldsymbol{\zeta}'_{ON} = \mathbf{K}(\theta)\delta\boldsymbol{\zeta}_{ON} \tag{41}$$

where $\mathbf{K}(\theta) \in \mathfrak{M}$, as $\mathbf{K}(\theta)$ contains only 2π-periodic trigonometric functions and $\mathbf{r}_N(\theta)$ and the perturbation force on the Keplerian reference orbit. According to the generalized averaging method (see Appendix B), if we find the solution to the generating function $\mathbf{U}(\theta)$ that satisfies

$$\mathbf{U} = \mathbf{K} + \mathbf{K}H_{\hat{\omega}_c}[\mathbf{U}] - H_{\hat{\omega}_c}[\mathbf{U}]L_{\hat{\omega}_c}[\mathbf{U}] \tag{42}$$

then we obtain the averaged system equation as

$$\delta\bar{\boldsymbol{\zeta}}'_{ON} = \mathbf{L}(\theta)\delta\bar{\boldsymbol{\zeta}}_{ON} \tag{43}$$

where $\mathbf{L} = L_{\hat{\omega}_c}[\mathbf{U}]$, and we denote $\delta\bar{\boldsymbol{\zeta}}_{ON}$ as the averaged state variable of $\delta\boldsymbol{\zeta}_{ON}$.

If we assume that $\mathbf{U}(\theta)$ has the same form as $\mathbf{K}(\theta)$, using Eqs. (35), (42), and (43), we get

$$\mathbf{L}(\theta) = L_{\hat{\omega}_c}[\mathbf{K}(\theta)] \tag{44}$$

where $\hat{\omega}_c = \min|1 + 2\varepsilon\hat{\omega}_{pm}|$. Equation (44) can be further calculated using Eq. (24) as

$$\begin{aligned}\mathbf{L}(\theta) &= \boldsymbol{\Xi}^{-1}(2\pi l)\begin{bmatrix}\delta\mathbf{A}_{\theta ON}(2\pi l) & \varepsilon\mathbf{b}_\theta(2\pi l)\\ \mathbf{0}_{1\times 6} & 0\end{bmatrix}\boldsymbol{\Xi}(2\pi l)\Big|_{l=\theta/2\pi} + \varepsilon\mathbf{C}^* \\ &= \begin{bmatrix}\boldsymbol{\Phi}_{\theta N}^{-1}\delta\mathbf{A}_{\theta ON}\boldsymbol{\Phi}_{\theta N} + \varepsilon\mathbf{C}_1^* & \varepsilon\boldsymbol{\Phi}_{\theta N}^{-1}\mathbf{b}_\theta + \varepsilon\mathbf{C}_2^*\\ \mathbf{0}_{1\times 6} & 0\end{bmatrix}\Big|_{l=\theta/2\pi}\end{aligned} \tag{45}$$

with certain constant matrices $\mathbf{C}^*$, $\mathbf{C}_1^*$, and $\mathbf{C}_2^*$. To solve Eq. (43) with the given coefficient matrix Eq. (45), we use the series expansion

$$\begin{aligned}\mathbf{L} &= \mathbf{L}_0 + \varepsilon\mathbf{L}_1 + \varepsilon^2\mathbf{L}_2 + \cdots \\ \delta\bar{\boldsymbol{\zeta}}_{ON} &= \delta\bar{\boldsymbol{\zeta}}_{ON0} + \varepsilon\delta\bar{\boldsymbol{\zeta}}_{ON1} + \varepsilon^2\delta\bar{\boldsymbol{\zeta}}_{ON2} + \cdots\end{aligned} \tag{46}$$

put it into Eq. (43) and equate the same-order terms for ε^i. The zeroth and first-order equations become

$$\begin{aligned}\delta\bar{\boldsymbol{\zeta}}'_{ON0} &= \mathbf{0} \\ \delta\bar{\boldsymbol{\zeta}}'_{ON1} &= \left\{\begin{bmatrix}\boldsymbol{\Phi}_{\theta N}^{-1}\delta\mathbf{A}_{\theta ON}\boldsymbol{\Phi}_{\theta N} & \varepsilon\boldsymbol{\Phi}_{\theta N}^{-1}\mathbf{b}_\theta\\ \mathbf{0}_{1\times 6} & 0\end{bmatrix}\Big|_{l=\theta/2\pi} + \varepsilon\mathbf{C}^*\right\}\delta\bar{\boldsymbol{\zeta}}_{ON0}\end{aligned} \tag{47}$$

From these, we can obtain the first-order solution for Eq. (43) under the initial condition given in Eq. (38) as

$$\delta\bar{\boldsymbol{\zeta}}_{ON}(\theta) = \begin{bmatrix}\mathbf{0}_{6\times 1}\\ 1\end{bmatrix} + \int_0^\theta\begin{bmatrix}(\mathbf{1} - \frac{s}{2\pi}\mathbf{W}_0)L_{\hat{\omega}_c}[\varepsilon\mathbf{b}_\theta(s)] + \varepsilon\mathbf{C}_2^*\\ 0\end{bmatrix}\mathrm{d}s \tag{48}$$

Because, from Eqs. (24) and (39),

$$\delta\bar{\boldsymbol{\xi}}_{ON}(\theta) = L_{\hat{\omega}_c}[\boldsymbol{\Xi}(\theta)\delta\bar{\boldsymbol{\zeta}}_{ON}(\theta)] = [\boldsymbol{\Xi}(2\pi n)\delta\bar{\boldsymbol{\zeta}}_{ON}(\theta)]_{n=\theta/2\pi} + \begin{bmatrix}\mathbf{c}_3^*\\ 0\end{bmatrix} \tag{49}$$

with a certain constant vector $\mathbf{c}_3^*$, Eq. (48) can be transformed to

$$\begin{aligned}\delta\bar{\boldsymbol{\xi}}_{ON}(\theta) &= \begin{bmatrix}\mathbf{0}_{6\times 1}\\ 1\end{bmatrix} \\ &+ \int_0^\theta\begin{bmatrix}(\mathbf{1} + \frac{1}{2\pi}(\theta - s)\mathbf{W}_0)L_{\hat{\omega}_c}[\varepsilon\mathbf{b}_\theta(s)] + \left(\mathbf{1} + \frac{\theta}{2\pi}\mathbf{W}_0\right)\varepsilon\mathbf{c}_3^*\\ 0\end{bmatrix}\mathrm{d}s\end{aligned} \tag{50}$$

The perturbation terms $\varepsilon\mathbf{b}_\theta(s)$ is assumed to be of the form Eq. (28) and its low-frequency part is given by Eq. (29). Therefore, the averaged relative motion $\delta\bar{\mathbf{x}}_{\theta ON}$, which is the first six elements of $\delta\bar{\boldsymbol{\xi}}_{ON}$ in Eq. (50), is obtained by performing the integration of the right-hand side of Eq. (50). For the purpose of this paper, we want to know only the functional form of it. Consequently, we can state that it takes the form

$$\begin{aligned}\delta\bar{\mathbf{x}}_{\theta ON}(\theta) = \varepsilon\Bigg[&\mathbf{p}_0 + \mathbf{p}_1\frac{\theta}{2\pi} + \mathbf{p}_2\left(\frac{\theta}{2\pi}\right)^2 + \sum_m\{\mathbf{p}_{cm}\cos\hat{\omega}_{pm}\theta \\ &+ \mathbf{p}_{sm}\sin\hat{\omega}_{pm}\theta\}\Bigg]\end{aligned} \tag{51}$$

where $\mathbf{p}_0$, $\mathbf{p}_1$, $\mathbf{p}_2$, $\mathbf{p}_{cm}$, and $\mathbf{p}_{sm}$ are constant vectors.

B. Averaged Monodromy Matrix for Relative Orbital Motion Between Two Spacecraft

Consider the averaged solution for the differential equation (with arbitrary initial condition) given in Eq. (16) (shown again next):

$$\delta\mathbf{x}'_{\theta PO} = \{\mathbf{A}_{\theta N}(\theta) + \delta\mathbf{A}_{\theta PO}(\theta)\}\delta\mathbf{x}_{\theta PO} \tag{52}$$

As it is already a homogeneous differential equation, we will go through similar manipulations as we did with Eqs. (39–51). By introducing the transformation

$$\delta\mathbf{x}_{\theta PO}(\theta) \triangleq \boldsymbol{\Phi}_{\theta N}(\theta, \theta_0)\delta\boldsymbol{\zeta}_{PO}(\theta) \tag{53}$$

where θ_0 is the true anomaly at an initial condition, Eq. (52) is transformed to the following differential equation with small coefficients:

$$\delta\boldsymbol{\zeta}'_{PO}(\theta) = \boldsymbol{\Phi}_{\theta N}^{-1}(\theta, \theta_0)\delta\mathbf{A}_{\theta PO}(\theta)\boldsymbol{\Phi}_{\theta N}(\theta, \theta_0)\delta\boldsymbol{\zeta}_{PO}(\theta) \tag{54}$$

where $\delta\mathbf{A}_{\theta PO}(\theta)$ is given in Eq. (17). We see from Eqs. (15) and (51) that $\delta\mathbf{A}_{\theta PO}(\theta)$ averaged over an orbital period takes the form

$$\begin{aligned}\delta\bar{\mathbf{A}}_{\theta PO}(\theta) = \varepsilon\Bigg[&\mathbf{A}_{\theta PO0} + \mathbf{A}_{\theta PO1}\frac{\theta}{2\pi} + \mathbf{A}_{\theta PO2}\left(\frac{\theta}{2\pi}\right)^2 \\ &+ \sum_m\{\mathbf{A}_{\theta POcm}\cos\hat{\omega}_{pm}\theta + \mathbf{A}_{\theta POsm}\sin\hat{\omega}_{pm}\theta\}\Bigg]\end{aligned} \tag{55}$$

where $\mathbf{A}_{\theta PO0}$, $\mathbf{A}_{\theta PO1}$, $\mathbf{A}_{\theta PO2}$, $\mathbf{A}_{\theta POcm}$, and $\mathbf{A}_{\theta POsm}$ are constant matrices, and $\delta\bar{\mathbf{A}}_{\theta PO}(\theta)$ is therefore of the order of ε.

By applying the generalized averaging method, we get the following averaged system equation:

$$\delta\bar{\boldsymbol{\zeta}}'_{PO} = \mathbf{L}(\theta)\delta\bar{\boldsymbol{\zeta}}_{PO} \tag{56}$$

where $\mathbf{L}(\theta)$ can be calculated as

$$\begin{aligned}\mathbf{L} &= L_{\hat{\omega}_c}[\boldsymbol{\Phi}_{\theta N}^{-1}(\theta, \theta_0)\delta\mathbf{A}_{\theta PO}(\theta)\boldsymbol{\Phi}_{\theta N}(\theta, \theta_0)] \\ &= \left(\mathbf{1} - \frac{\theta - \theta_0}{2\pi}\mathbf{W}(\theta_0)\right)\delta\bar{\mathbf{A}}_{\theta PO}(\theta)\left(\mathbf{1} + \frac{\theta - \theta_0}{2\pi}\mathbf{W}(\theta_0)\right) + \varepsilon\mathbf{C}^*\end{aligned} \tag{57}$$

In Eq. (57), $\hat{\omega}_c = \min|1 + 2\varepsilon\hat{\omega}_{pm}|$, and $\mathbf{C}^*$ is a certain constant matrix.

By following the procedure used for Eq. (46), we get the first-order solution for Eq. (56) as

$$\begin{aligned}\delta\bar{\boldsymbol{\zeta}}_{PO}(\theta) = \mathbf{1} + \int_{\theta_0}^\theta\Bigg\{&\left(\mathbf{1} - \frac{s}{2\pi}\mathbf{W}_0\right)\delta\bar{\mathbf{A}}_{\theta PO}(s)\left(\mathbf{1} + \frac{s}{2\pi}\mathbf{W}_0\right) \\ &+ \varepsilon\mathbf{C}^*\Bigg\}\,\mathrm{d}s \bullet \delta\bar{\boldsymbol{\xi}}_{PO}(\theta_0)\end{aligned} \tag{58}$$

From Eqs. (53), (55), and (57), we obtain the form of $\delta\bar{\mathbf{x}}_{\theta PO}$ as

$$\delta\bar{\mathbf{x}}_{\theta PO}(\theta) = \left(\mathbf{1} + \frac{\theta-\theta_0}{2\pi}\mathbf{W}(\theta_0)\right) \times \left[\mathbf{1} + \int_{\theta_0}^{\theta}\left\{\left(\mathbf{1} - \frac{s}{2\pi}\mathbf{W}_0(\theta_0)\right)\delta\bar{\mathbf{A}}_{\theta PO}(s) \times \left(\mathbf{1} + \frac{s}{2\pi}\mathbf{W}(\theta_0)\right) + \varepsilon\mathbf{C}^*\right\}\mathrm{d}s\right]\delta\mathbf{x}_{\theta PO}(\theta_0) \tag{59}$$

The coefficient matrix appearing in Eq. (59) is the desired state transition matrix averaged over each orbital period:

$$\bar{\mathbf{\Phi}}_{\theta P}(\theta,\theta_0) = \left(\mathbf{1} + \frac{\theta-\theta_0}{2\pi}\mathbf{W}(\theta_0)\right)\left[\mathbf{1} + \int_{\theta_0}^{\theta}\left\{\left(\mathbf{1} - \frac{s}{2\pi} \times \mathbf{W}(\theta_0)\right)\delta\bar{\mathbf{A}}_{\theta PO}(s)\left(\mathbf{1} + \frac{s}{2\pi}\mathbf{W}(\theta_0)\right) + \varepsilon\mathbf{C}^*\right\}\mathrm{d}s\right] \tag{60}$$

From Eqs. (55) and (60), the averaged state transition matrix for one orbital period, to the first order, is found to take the form

$$\mathbf{M}(n,\theta_0) \triangleq \bar{\mathbf{\Phi}}_{\theta P}(2(n+1)\pi+\theta_0, 2n\pi+\theta_0) = (\mathbf{1}+\mathbf{W}(\theta_0))\left[\mathbf{1} + \varepsilon\left\{\sum_{m=0}^{l_P}(\mathbf{M}_{pm}(\theta_0)n^m) + \sum_{m=1}^{l_S}(\mathbf{M}_{cm}(\theta_0)\cos 2\pi\hat{\omega}_{pm}n + \mathbf{M}_{sm}(\theta_0)\sin 2\pi\hat{\omega}_{pm}n)\right\}\right] \tag{61}$$

where n is an integer orbital revolution number; $\mathbf{M}_{pm}$, $\mathbf{M}_{cm}$, and $\mathbf{M}_{sm}$ are all 6×6 constant matrices (for a fixed θ_0); and l_P and l_S are the maximum order of polynomial and sinusoidal terms, respectively. From Eqs. (55) and (60), we see analytically that $l_P = 2$ and l_S is infinity. $\mathbf{W}$ is defined in Eq. (A16).

Equation (61) provides a convenient form for curve-fitting, in which $\mathbf{W}(\theta_0)$ is determined from Keplerian elements (osculating orbital elements) at the initial epoch $\theta = \theta_0$, and the parameters $\mathbf{M}_{pm}$, $\mathbf{M}_{cm}$, and $\mathbf{M}_{sm}$ can be determined using data from high-fidelity orbit propagators. Because it can incorporate all the perturbation terms with a time constant longer than the orbital period, it is expected to model the averaged solution of first-order orbital motion over a long duration.

C. Approximate Relation Between Time and True Anomaly

So far, we used the true anomaly as the dependent variable. It is useful, however, to choose time as the dependent variable for practical applications. For example, spacecraft onboard systems usually know the current time immediately by onboard clocks, but to obtain the true anomaly requires some sort of orbit calculation using their current position information.

The relation between the mean anomaly M_O of the perturbed reference orbit $(\mathbf{r}_O^I, \dot{\mathbf{r}}_O^I)$ and the time is given by the following Gauss's planetary equation for mean anomaly:

$$\frac{\mathrm{d}M_O(t)}{\mathrm{d}t} = \omega_N + \frac{b}{\omega_N a^2 be}\left[\left(\frac{b^2}{a}\cos\theta_N - 2r_N(\theta_N)e\right)\bullet\varepsilon f_{Nr}(\theta_N) - \left(\frac{b^2}{a} + r_N(\theta_N)\right)\sin\theta_N \bullet \varepsilon f_{N\theta}(\theta_N)\right] \tag{62}$$

where a, b, ω_N, e, and θ_N are the semimajor axis, semiminor axis, natural frequency, eccentricity, and true anomaly of the reference (Keplerian) orbit, respectively; εf_{Nr} and $\varepsilon f_{N\theta}$ are the perturbation forces along the radial direction and tangential direction. As we see from Eq. (62) that the right-hand side of the equation is of the form of $\mathfrak{M}$ given in Eq. (18) with no secular terms, the averaged behavior of the true anomaly can be written as

$$\bar{\theta}_O(t) = L_{\hat{\omega}_c}[\theta_O(t)] = L_{\hat{\omega}_c}[M_O(t)] = \omega_N t + \varepsilon\left[\rho_0 + \rho_1 t + \sum_m\{\rho_{cm}\cos\varepsilon\omega_{pm}t + \rho_{sm}\sin\varepsilon\omega_{pm}t\}\right] \tag{63}$$

where we assume $\hat{\omega}_c = \min|1 + 2\varepsilon\hat{\omega}_{pm}|$, $\varepsilon\omega_{pm}$ is the angular frequency of the perturbation force, and ρ_0, ρ_1, ρ_{cm}, and ρ_{sm} are constant parameters.

As we have derived in the previous sections, the behavior of the follower satellite linearized around the leader satellite (although it is expressed using the two-body reference orbit information), the true anomaly appearing as the dependent parameters of the approximate state transition matrix Eq. (61), should actually be $\theta_O(t)$. Therefore, one should use Eq. (63) to obtain the true anomaly from the time. The normalized angular frequency of perturbation forces $\varepsilon\hat{\omega}_{pm}$ appearing in the previous sections [e.g., in Eq. (61)] should also be normalized using Eq. (63). Specifically, it becomes

$$\varepsilon\hat{\omega}_{pm} = \frac{\varepsilon\omega_{pm}}{(\mathrm{d}/\mathrm{d}t)(\bar{\theta}_O)} \approx \frac{\varepsilon\omega_{pm}}{\omega_N + \varepsilon\theta_1} \tag{64}$$

D. Approximate State Transition Matrix Between Arbitrary Times

By using Eq. (61), the averaged state transition matrix after n revolutions can be obtained as follows:

$$\bar{\mathbf{\Phi}}_{\theta P}(2\pi n+\theta_0,\theta_0) = \mathbf{M}(n-1,\theta_0)\bullet\cdots\bullet\mathbf{M}(1,\theta_0)\bullet\mathbf{M}(0,\theta_0) = \prod_{k=0}^{n-1}\mathbf{M}(k,\theta_0) \tag{65}$$

Because Eq. (65) provides a state transition matrix averaged over one orbital period, it contains effects of all terms slower than the orbital period. As we consider the orbital dynamics, the remaining terms that are not taken into account in Eq. (65) are all periodic functions containing only an integer-multiple frequency of the orbital frequency. Thus,

$$\mathbf{\Phi}_{\theta P}(2n\pi+\theta_0+\Delta\theta,\theta_0) = \sum_{k=1}^{l_I}[\mathbf{N}_{ck}(\theta_0)\cos k\Delta\theta + \mathbf{N}_{sk}(\theta_0)\sin k\Delta\theta] + \prod_{k=0}^{n-1}\mathbf{M}(k,\theta_0) \tag{66}$$

where $0 \le \Delta\theta < 2\pi$, $\mathbf{N}_{ck}$ and $\mathbf{N}_{sk}$ are 6×6 constant matrices (for a fixed θ_0) corresponding to coefficients of the Fourier series, and l_I is the maximum order of the Fourier coefficients to be considered.

E. Outline of Parameters Determination Process

As shown in Eq. (66), the total number of 6×6 coefficient matrices q is given by

$$q = q_I + q_A \tag{67}$$

where

$$q_I = 2l_I, \qquad q_A = l_P + 1 + \sum_{i=1}^{N} 2l_{Si}$$

where N is a number of periodic perturbation sources to be considered. Therefore, there are $36q$ parameters to be determined by the following parameter-determination process.

For this purpose, let us introduce the matrix vectorization operator defined as

$$\mathrm{vec}\,\mathbf{A} = [a_{11}a_{21}\cdots a_{n1}a_{12}a_{22}\cdots a_{nm}]^T \quad \text{for } \mathbf{A} = \{a_{ij}\} \in R^{n\times m} \tag{68}$$

Equation (61) can be reformulated in the following form:

$$\mathrm{vec}\,\mathbf{M}(n,\theta_0) = \mathbf{F}(n;\theta_0)\cdot\mathbf{p}_A(\theta_0) \tag{69}$$

where $\mathbf{p}_A(\theta_0)$ is a $36q_A\times 1$ column vector for which the elements are composed of each element of $\mathbf{M}_{pm}$, $\mathbf{M}_{cm}$, and $\mathbf{M}_{sm}$: that is,

$$\mathbf{p}_A(\theta_0) = [\{\mathrm{vec}\mathbf{M}_{p0}(\theta_0)\}^T, \{\mathrm{vec}\mathbf{M}_{p1}(\theta_0)\}^T, \ldots, \{\mathrm{vec}\mathbf{M}_{c1}(\theta_0)\}^T, \ldots, \{\mathrm{vec}\mathbf{M}_{s1}(\theta_0)\}^T, \ldots]^T \tag{70}$$

$\mathbf{F}(n;\theta_0)$ is a $36 \times 36q_A$ matrix to equalize Eqs. (61) and (69). This is always possible because the approximate monodromy matrix given by Eq. (61) is linear in terms of the parameter matrices $\mathbf{M}_{pm}$, $\mathbf{M}_{cm}$, and $\mathbf{M}_{sm}$.

One of the simplest ways to determine $\mathbf{p}_A$ is to apply the least-squares method:

$$\mathbf{p}_A = \left[\sum_n \mathbf{F}(n;\theta_0)^T\mathbf{F}(n;\theta_0)\right]^{-1}\left[\sum_n \mathbf{F}(n;\theta_0)^T\mathrm{vec}\mathbf{M}^{(\mathrm{real})}(n;\theta_0)\right] \tag{71}$$

where we denote $\mathbf{M}^{(\mathrm{real})}$ as the real data of $\mathbf{M}$ obtained by high-fidelity orbit propagation. Thus, $\mathbf{M}^{(\mathrm{fit})}$, an estimated value of $\mathbf{M}$, can be obtained by rearranging each element of $\mathbf{p}_A$ by the inverse operation of Eq. (70) and applying Eq. (61).

The parameter matrices within one orbital period, $\mathbf{N}_{ck}$ and $\mathbf{N}_{sk}$, can be determined by substituting the estimated monodromy matrix $\mathbf{M}^{(\mathrm{fit})}$ and the real data of the state transition matrix $\mathbf{\Phi}_{\theta P}^{(\mathrm{real})}$ into Eq. (66):

$$\mathbf{\Phi}_{\theta P}^{(\mathrm{real})}(2n\pi + \theta_0 + \Delta\theta, \theta_0) - \prod_{k=0}^{n-1}\mathbf{M}^{(\mathrm{fit})}(k,\theta_0) = \sum_{k=1}^{l_I}[\mathbf{N}_{ck}(\theta_0)\cos k\Delta\theta + \mathbf{N}_{sk}(\theta_0)\sin k\Delta\theta] \tag{72}$$

In Eq. (72), the right-hand side of the equation contains unknown parameters to be determined, and the left-hand side of the equation is given. Therefore, in the same way as we did in Eqs. (69–71), the least-squares estimate of $\mathbf{N}_{ck}$ and $\mathbf{N}_{sk}$ can be obtained.

F. Optimum Phase for Parameters Determination

When determining the parameters in Eq. (66), we have freedom to choose the phase θ_0, which leaves room for optimization. To search for the optimum phase, let us simplify in such a way that the state transition matrix within one orbital period is approximated by the Keplerian dynamics. In this case, the relative state vector is calculated from Eq. (66) as

$$\delta\mathbf{x}_{\theta PO}(2n\pi + \theta_0 + \Delta\theta) \approx \mathbf{\Phi}_{\theta P}(2n\pi + \theta_0 + \Delta\theta, \theta_0)\delta\mathbf{x}_{\theta PO}(\theta_0) = \mathbf{\Phi}_{\theta N}(\theta_0 + \Delta\theta, \theta_0)\prod_{k=0}^{n-1}\mathbf{M}(k,\theta_0)\delta\mathbf{x}_{\theta PO}(\theta_0) = \mathbf{\Phi}_{\theta N}(2n\pi + \theta_0 + \Delta\theta, \theta_0)\{\delta\mathbf{x}_{\theta PO}(\theta_0) + \varepsilon\mathbf{G}(n;\theta_0, \delta\mathbf{x}_{\theta PO}(\theta_0))\mathbf{p}_A(\theta_0)\} \tag{73}$$

where $\mathbf{p}_A(\theta_0)$ is a $36q_A \times 1$ estimation parameters vector defined in Eq. (69), and $\varepsilon\mathbf{G}$ is a $6 \times 36q_A$ coefficient matrix to appropriately complete Eq. (73). This is always possible because the approximate monodromy matrix is linear in terms of $\mathbf{p}_A$. Equation (73) explicitly relates the estimation parameters vector $\mathbf{p}_A$ with the state vector at an arbitrary true anomaly. The error in the state vector due to the estimation error in $\mathbf{p}_A$ is measured by the covariance matrix. To know the covariance matrix for an arbitrary time, let us put $\theta = 2n\pi + \theta_0 + \Delta\theta$ and denote $\sigma(\theta_0)$ as the deviation of $\varepsilon\mathbf{G}\mathbf{p}_A$ (corresponding to the fitting error, assuming a uniform and independent event). Then the covariance matrix of $\delta\mathbf{x}_{\theta PO}(\theta)$, denoted by $\mathbf{\Psi}(\theta)$, becomes

$$\mathbf{\Psi}(\theta) \approx \mathbf{\Phi}_{\theta N}(\theta,\theta_0)\mathbf{\Phi}_{\theta N}(\theta,\theta_0)^T\sigma(\theta_0)^2 \tag{74}$$

where $\mathbf{\Psi}(\theta)$ provides an index of how the fitting inaccuracy affects the accuracy of the propagation of state vectors. In Eq. (74), $\mathbf{\Phi}_{\theta N}\mathbf{\Phi}_{\theta N}^T$ can be considered as a scale factor to be multiplied to the fitting error. Hence, the optimum phase that minimizes the growth rate of the propagation error due to the fitting error can be obtained when the following function is minimized:

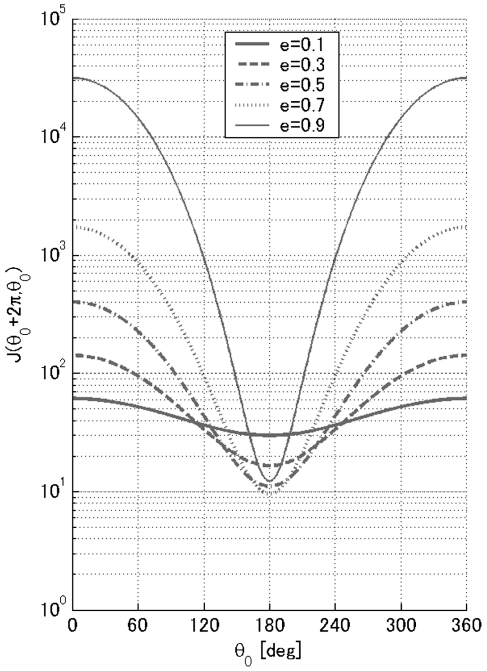

Fig. 1 Propagations of estimation error after one revolution with different initial true anomaly.

$$J(\theta,\theta_0) = \sqrt{\mathrm{tr}[\mathbf{\Phi}_{\theta N}(\theta,\theta_0)\mathbf{\Phi}_{\theta N}(\theta,\theta_0)^T]} \tag{75}$$

Figure 1 shows $J(2\pi + \theta_0, \theta_0)$ for various-eccentricity orbits. In all cases, $J(2\pi + \theta_0, \theta_0)$ is minimized at apoapsis (which implies that the best state transition matrix data for curve-fitting are those at apoapsis) and is especially crucial for high-eccentricity orbits. If we choose apoapsis data, then the magnification factor of the fitting errors after one orbital period is around 10, whereas if we choose periapsis data, the factor becomes worse by up to four orders of magnitude. Therefore, it is important to choose apoapsis data as a source for curve-fitting for long-term evaluations of relative orbital motions.

Figure 2 shows the propagation of the fitting error for up to 10 orbital revolutions when using periapsis and apoapsis data [$J(\theta, 0)$ and $J(\theta, \pi)$]. As is seen from these figures, the propagated error is proportional to time in both cases. However, as is also implied from Fig. 1, their slopes vary widely. Again, we see that using apoapsis

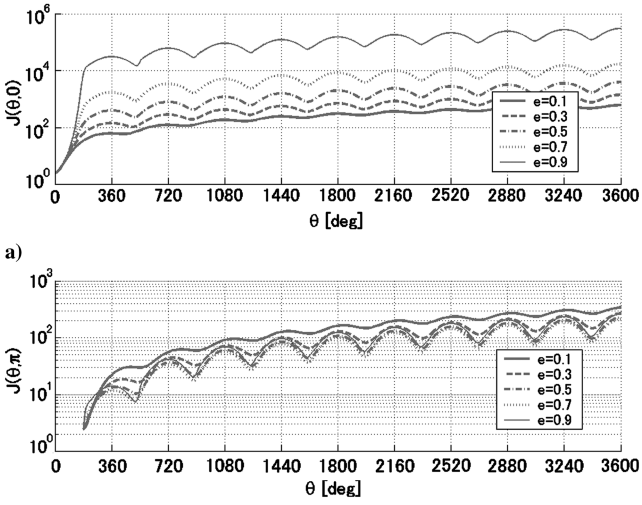

Fig. 2 Propagations of estimation error for 10 rev performed at a) periapsis ($\theta_0 = 0$) and b) apoapsis ($\theta_0 = \pi$).

state transition matrix data is optimal for minimizing the effect of the estimation error with a given fitting performance.

IV. Numerical Validations

A. Performance for Typical Formation-Flying Orbit

To use the approximate state transition matrix proposed in the previous sections, the source information of state transition matrices, to which the approximate state transition matrix is going to be fitted, is required. The source information must be accurate, and hence it is assumed to be generated by a high-fidelity orbit propagator. For the evaluations in this paper, we generate this source matrix data by a numerical-symplectic state transition matrix derived in [20]. Perturbations incorporated in the source matrix data include the geopotential terms of the Earth up to the (degree, order) of (5,5) and the third-body gravitational effect of the sun and the moon throughout this paper.

The performance of the approximate state transition matrix is evaluated for Earth orbits using the following specific form, derived from Eqs. (61) and (66):

$$\begin{aligned}\boldsymbol{\Phi}_{\theta P}(2(n+1)\pi+\theta_0+\Delta\theta, 2n\pi+\theta_0) &= (\mathbf{1}+\mathbf{W}(\theta_0))\\ &\times\left[\mathbf{1}+\varepsilon\sum_{m=0}^{l_P}(\mathbf{M}_{pm}(\theta_0)n^m)+\varepsilon\sum_{m=1}^{l_{S1}}(\mathbf{M}_{1cm}(\theta_0)\cos 2\pi m\hat{\omega}_{p1}n\right.\\ &+\mathbf{M}_{1sm}(\theta_0)\sin 2\pi m\hat{\omega}_{p1}n)+\varepsilon\sum_{m=1}^{l_{S2}}(\mathbf{M}_{2cm}(\theta_0)\cos 2\pi m\hat{\omega}_{p2}n\\ &+\mathbf{M}_{2sm}(\theta_0)\sin 2\pi m\hat{\omega}_{p2}n)+\varepsilon\sum_{m=1}^{l_I}[\mathbf{N}_{cm}(\theta_0)\cos m\Delta\theta\\ &\left.+\mathbf{N}_{sm}(\theta_0)\sin m\Delta\theta]\right] \qquad (76)\end{aligned}$$

where $\hat{\omega}_{p1}$ and $\hat{\omega}_{p2}$ are the angular velocities of the sun and the moon normalized by the orbital angular velocity with the correction based on Eq. (64). By the form Eq. (76), the geopotential perturbation effect in the source matrix data is to be absorbed by the polynomial terms (the first summation term in the large bracket), whereas the sun's and moon's perturbation effects are to be absorbed by both the polynomial terms and the corresponding sinusoidal terms (the second and third summation terms). The fourth summation term in Eq. (76) corresponds to the interpolation term.

The variables l_P, l_{S1}, l_{S2}, and l_I in Eq. (76) are the order of approximations for the polynomial, the sun's and moon's sinusoidal terms, and the terms for an interpolation between one orbital revolution, respectively. Various combinations of approximation orders $(l_P, l_{S1}, l_{S2}, l_I)$ are possible to achieve a desired performance. Some example combinations of approximation orders and the resulting number of parameters to be fitted are shown in Table 1. The total number of variables in Table 1 is calculated through $36q$, where q is defined in Eq. (67). The last two cases (p2s2m4-symp1 and p2s2m4-symp2) are the results of the parameter reduction using a mathematical structure of the state transition matrix, and they are discussed in detail in the next section.

Table 2 shows the orbit parameters of the leader satellite and the follower satellite to be used for the following performance evaluations. Two orbits are selected to have identical semimajor axes, which means that if there are no perturbations, the relative motion of the two spacecraft would be periodic. In reality, due to the presence of perturbation forces, the relative motion is not periodic and is shown in Fig. 3.

Figure 4 shows results of the curve-fitting for the case p2s2m4. In this case, the interpolation terms are omitted and the graphs are plotted with one orbital-period step with the data at each apogee. The fitting span is chosen to be 90 orbital revolutions. Figure 4a shows the true-anomaly deflection from that calculated by the corresponding Keplerian dynamics. It shows an almost linear behavior, which supports the validity of Eq. (63). Figure 4b shows the fitting quality of the curve-fitting, evaluated by

$$\text{fitting quality} = \frac{\|\mathbf{M}(n,\theta_0)^{(\text{fit})}-\mathbf{M}(n,\theta_0)^{(\text{real})}\|}{\|\mathbf{M}(n,\theta_0)^{(\text{real})}\|} \qquad (77)$$

It can be seen that the fitting quality is flat and is not deteriorated thorough the 90 revolutions of the fitting span, which indicates that the functional form in Eq. (76) is well suited for the perturbed state transition matrix over a long duration. The fitting error outside the fitting span is observed to grow worse. This is because the fitting is optimized only for the fitting span (of 90 revolutions in this case.)

Figure 4c is the positional error for the orbital parameters shown in Table 2. The error is evaluated according to

$$\text{positional error} = \frac{\|\mathbf{r}(t)^{(\text{true})}-\mathbf{r}(t)^{(\text{fit})}\|}{\|\mathbf{r}(t)^{(\text{true})}\|} \qquad (78)$$

The error here is the difference between the relative positions calculated by the source matrix data and the fitted matrix data. We see

Table 1 Test cases for numerical validations and its relation to the number of parameters

Case ID	Approximation Order				Number of Matrix				Total no of variables
	Polynomial l_P	Sun freq. l_{S1}	Moon freq. l_{S2}	Interpolation l_I	Polynomial $\mathbf{M}_p$	Sun freq. $\mathbf{M}_{1s}$, $\mathbf{M}_{1c}$	Moon freq. $\mathbf{M}_{2s}$, $\mathbf{M}_{2c}$	Interpolation $\mathbf{N}_s$, $\mathbf{N}_c$	
p0s0m0	0	0	0	——	1	0	0	0	36
p2s0m0	2	0	0	——	3	0	0	0	108
p2s0m1	2	0	1	——	3	0	2	0	180
p2s0m2	2	0	2	——	3	0	4	0	252
p2s2m2	2	2	2	——	3	2	4	0	324
p2s2m4	2	2	4	——	3	4	8	0	540
p2s2m4i4	2	2	4	4	3	4	8	8	828
p2s2m4-symp1	2	2	4	——	3	4	8	0	225
p2s2m4-symp2	2	2	4	——	3	4	8	0	225

Table 2 Orbital elements for performance test[a]

	a, km	e	i, deg	Ω, deg	ω, deg	θ, deg
Leader	89,292	0.4	30	0	0	180
Follower	89,292	0.40000969	30	0	−0.001604	−179.998625

[a]Orbital epoch is 1 Jan. 2010 at 0000 hrs Coordinated Universal Time and the initial spacecraft distance is 1000 m at apogee.

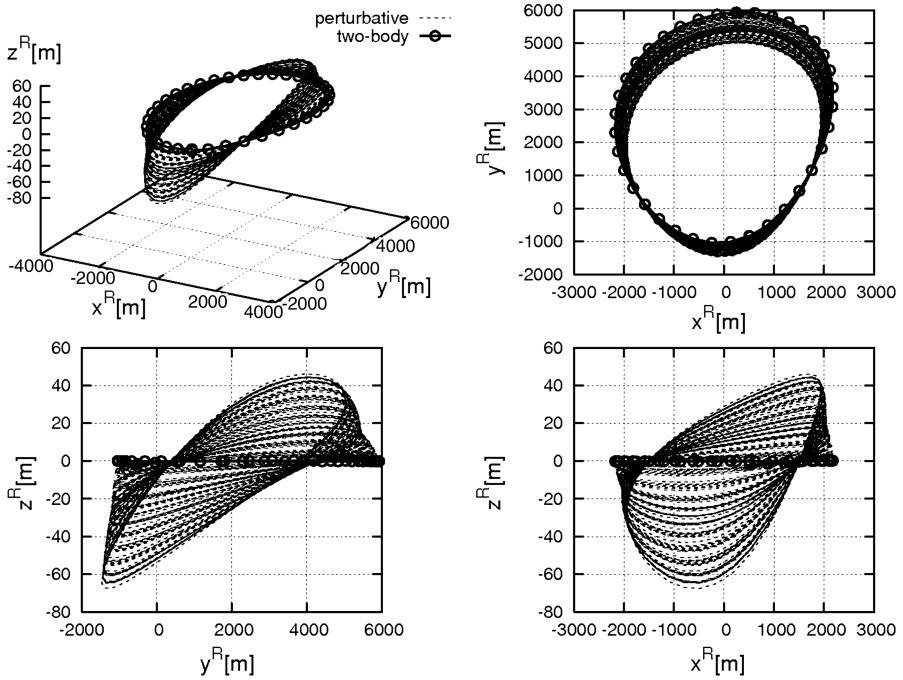

Fig. 3 Example of relative motion in an elliptic orbit with and without perturbation effects, drawn in a rotating coordinate frame. Orbital parameters of this drawing are shown in Table 2.

that 0.1–1% accuracy is achieved. Figure 4d is the error between the positions calculated directly by the source matrix data and by the fitted matrix data. Because the real orbital behavior is nonlinear, the calculation based on the source matrix data still has an error due to the linearization. Therefore, Fig. 4c shows the error due to the fitting performance, and Fig. 4d shows the overall error including the fitting performance and the effect of nonlinearity. The important point here is that we see from Fig. 4d that the fitted data align well with the real data, which implies that the fitting error is less than the nonlinearity error. Therefore, the approximate state transition matrix for this typical case can be said to be practical and useful.

Figure 5 shows the case p2s2m2i4, which simply adds the interpolation terms to p2s2m2. Figure 5a shows the fitting quality as a function of the true anomaly. To see the fitting quality of the interpolation terms, all the data for 90 revolutions are plotted modulo 360 deg. The graph shows that the systematic error is dominant rather than the random error. This implies that higher-order interpolation terms would improve fitting quality. Figure 5b is the positional error, which corresponds to Fig. 4c with denser data (the data between one orbital period are added). The error magnitude is worst around perigee, due the magnification effect of the propagation, which is basically the same reason as discussed in Sec. III.F. Nevertheless, the error is bounded throughout 90 revolutions, providing a flat level of positional error throughout the fitting span.

B. Performance for Various Approximation Orders

Performance variations for several combinations of approximation orders are evaluated using the orbital data in Table 2. Figure 6 shows the error between fitted data and the real (nonlinear) data. The relative position calculated based on a two-body (Keplerian) dynamics is also plotted for comparison. The source data in Fig. 6, which are calculated with the source matrix data, provide the theoretical minimum. The figure indicates that the Keplerian dynamics cannot achieve sufficient accuracy, as the curve for it always shows double-digit larger error than the curve for the source data. By adding more approximation terms, it is improved to almost align with the source data. For this orbit, second-order terms for polynomial and sinusoidal terms seem sufficient.

C. Performance for Various Eccentricity

The approximate state transition matrix is applied to various-eccentricity orbits. The orbital parameters chosen for the evaluation are based on Table 2, except for the eccentricity. The results are

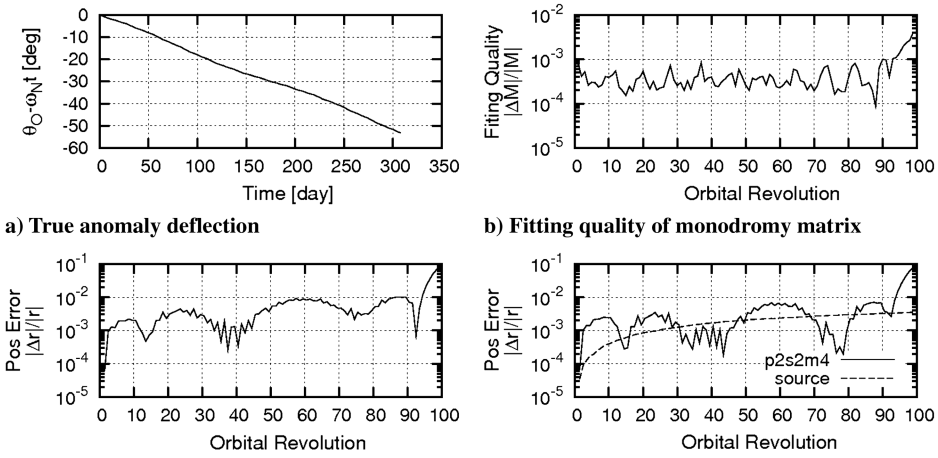

a) True anomaly deflection **b) Fitting quality of monodromy matrix**

c) Positional error from the source data **d) Positional error from the real orbit**

Fig. 4 Example of fitting performance.

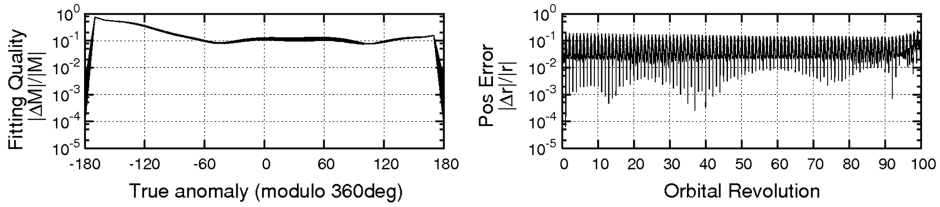

a) Fitting quality of interpolation within 1 rev **b) Positional error from the source data**

Fig. 5 Example of interpolation within one orbital period.

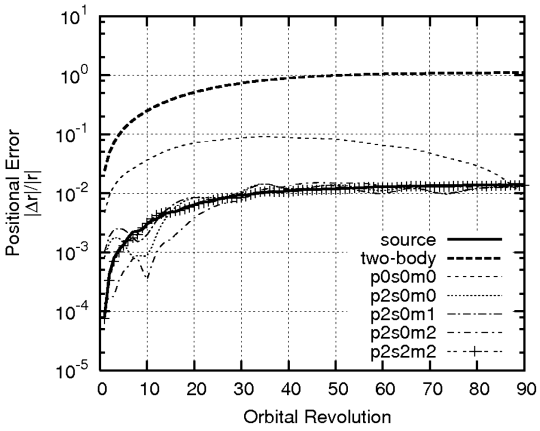

Fig. 6 Positional accuracy for various approximation orders.

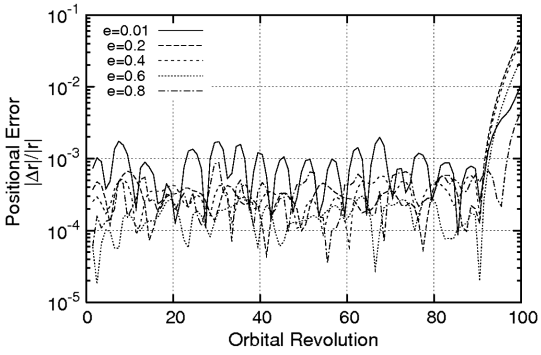

Fig. 7 Positional accuracy for various-eccentricity orbits.

shown in Fig. 7. As can be seen from this figure, the positional error does not differ as much as the eccentricity is changed. This indicates that the functional form of Eq. (76) covers a wide range of orbital shapes without deteriorating its fitting performance.

D. Performance for Various Semimajor Axis

The approximate state transition matrix is applied to various semimajor-axis orbits. The orbital parameters chosen for the evaluation are based on Table 2, except for the semimajor axis. As is indicated by Eq. (32), the applicability of the generalized averaging method is limited by the relation between an orbital period and the period of the sun and the moon. The fitting performance is expected to deteriorate as the spectrum of the Keplerian orbital behavior gets close to or overlaps with those of the sun and the moon. Equation (32) suggests that the perturbation sources that have a closer frequency to the Keplerian orbit frequency have a stronger effect, which is the moon for general Earth orbits. From Eq. (32), the following condition is derived:

$$T < \frac{T_{\text{moon}}}{2n_{\text{moon}}} \tag{79}$$

where $n_{\text{moon}} \triangleq \max(l_{S2})$ and T is the orbital period. This provides a rough guide to the maximum orbital period for which the approximate state transition matrix is valid, when the n_{moon}th-order sinusoidal terms of the moon's perturbation is not negligible.

Figure 8 shows the average fitting quality and the variance of the positional error in the 90-revolution fitting span. As expected from the preceding discussions, the error increases as the semimajor axis increases. The limitations derived by Eq. (79) are also plotted for $n_{\text{moon}} = 2, 3, 4$. From Fig. 8b, it can be seen that 1% positional accuracy is achieved for orbits with up to 10-Earth-radii semimajor axes. This, of course, covers low Earth orbit (LEO), geosynchronous orbits, and equivalent-period orbits with arbitrary eccentricities.

V. Parameter Reduction Using the Symplectic Structure of the State Transition Matrix

This section considers a fundamental mathematical structure that state transition matrices for any Hamiltonian system possess by nature. Symplecticity is one such mathematical structure. Because symplecticity is a direct outcome of a Hamiltonian formulation, preserving symplectic structure provides an important feature for Hamiltonian system, such as conservations of the energy and angular momentum, and even eigenstructure. A typical example of the importance of the symplectic property for state transition matrices in astrodynamics is found in [23–25], in which it is shown that the propagation of orbit uncertainty has certain constraints and properties that arise from the symplectic form of the state transition matrix. Thus, it is important to maintain these properties when mapping orbit uncertainty. It also provides some nice properties for practical numerical manipulation [20].

A. Symplectic Structure of a Hamiltonian System

Let us limit discussions hereafter to the case in which the dynamics we deal with are subject to Hamiltonian mechanics. This implies that we consider third bodies and higher-order gravitational potential, but any dissipation forces such as atmospheric drag are out of scope for the following discussions.

It is well known that the state transition matrix for any Hamiltonian system $\mathbf{\Phi}$ is symplectic: that is,

$$\mathbf{\Phi}^T \mathbf{J} \mathbf{\Phi} = \mathbf{J} \tag{80}$$

where

$$\mathbf{J} = \begin{bmatrix} \mathbf{0}_{3\times3} & \mathbf{1}_{3\times3} \\ -\mathbf{1}_{3\times3} & \mathbf{0}_{3\times3} \end{bmatrix} \tag{81}$$

is called the symplectic basis. Note that $\mathbf{J}$ has the following special properties:

$$\mathbf{J}^2 = -\mathbf{1}_{3\times3}, \qquad \mathbf{J}^T\mathbf{J} = \mathbf{1}_{3\times3}, \qquad \mathbf{J}^T = -\mathbf{J}, \qquad |\mathbf{J}| = 1 \tag{82}$$

It can easily be derived from Eqs. (80) and (82) that if $\mathbf{\Phi}_1$ and $\mathbf{\Phi}_2$ are symplectic, then $\mathbf{\Phi}_1\mathbf{\Phi}_2$ is also symplectic. We can also get the following symplectic inverse formula from these equations:

$$\mathbf{\Phi}^{-1} = \mathbf{J}^{-1}\mathbf{\Phi}^T\mathbf{J} = -\mathbf{J}\mathbf{\Phi}^T\mathbf{J} \tag{83}$$

These properties are important mathematical structures and show that symplectic matrices form a group. They are also useful for practical numerical computations when using state transition matrices.

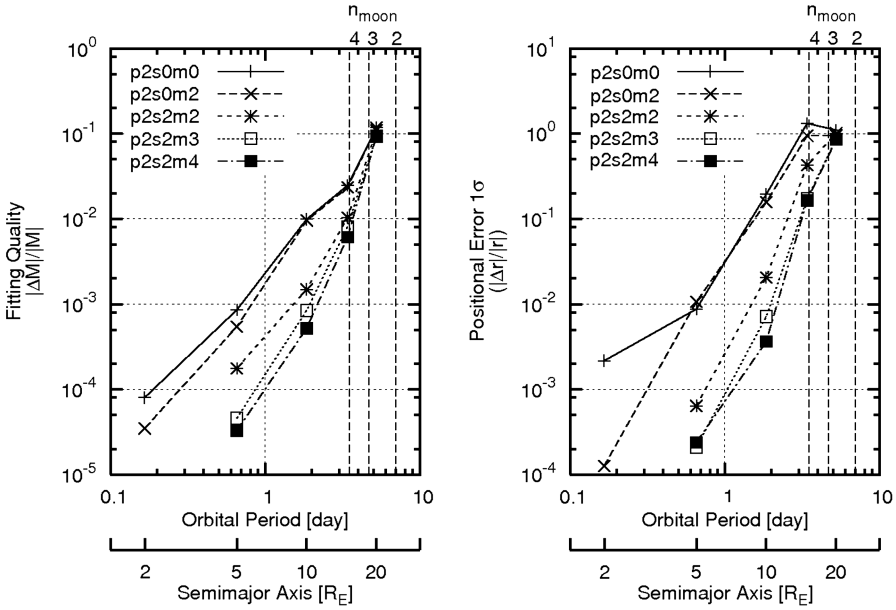

Fig. 8 Positional accuracy for various semimajor-axis orbits.

Let λ and $\boldsymbol{\mu}$ denote the eigenvalue and eigenvector of the state transition matrix $\boldsymbol{\Phi}$, respectively. They satisfy

$$\boldsymbol{\Phi}\,\boldsymbol{\mu} = \lambda\boldsymbol{\mu} \tag{84}$$

Hence,

$$\boldsymbol{\mu}^T\boldsymbol{\Phi}^T = \lambda\boldsymbol{\mu}^T \Rightarrow \lambda\boldsymbol{\mu}^T\mathbf{J}\boldsymbol{\Phi} = \boldsymbol{\mu}^T\boldsymbol{\Phi}^T\mathbf{J}\boldsymbol{\Phi} = \boldsymbol{\mu}^T\mathbf{J}$$

and consequently,

$$(\boldsymbol{\mu}^T\mathbf{J})\boldsymbol{\Phi} = \lambda^{-1}(\boldsymbol{\mu}^T\mathbf{J}) \tag{85}$$

where $\boldsymbol{\mu}^T\mathbf{J}$ and λ^{-1} are seen to be the left eigenvector and eigenvalue of $\boldsymbol{\Phi}$, respectively. Therefore, if $\boldsymbol{\Phi}$ is a real matrix, and if one of the eigenvalues is λ, then λ^{-1}, λ^*, and λ^{*-1} are also eigenvalues of $\boldsymbol{\Phi}$, where λ^* denotes a conjugate of λ. This property induces the following equality:

$$\det\boldsymbol{\Phi} = \prod_i \lambda_i = 1 \tag{86}$$

B. Conditions to Preserve Symplectic Structure

Let us write the monodromy matrix in the following compact form:

$$\mathbf{M}(n,\theta_0) = \boldsymbol{\Phi}_{\theta N}(\theta_0+2\pi,\theta_0)[\mathbf{1}+\varepsilon\mathbf{M}_1(n,\theta_0) + \varepsilon^2\mathbf{M}_2(n,\theta_0)+\cdots] \tag{87}$$

where $\varepsilon^i\mathbf{M}_i$ represents the ith-order terms of ε. If we consider up to first order, Eq. (87) is equivalent to Eq. (61) [$\mathbf{M}_1$ corresponds to the summation of the terms attached to parameter matrices $\mathbf{M}_{pm}$, $\mathbf{M}_{cm}$, and $\mathbf{M}_{sm}$ in Eq. (61)]. Note that if $\boldsymbol{\Phi}_N(\theta_0+2\pi,\theta_0)$ is symplectic, $\boldsymbol{\Phi}_{\theta N}(\theta_0+2\pi,\theta_0)$ is also symplectic, because

$$\boldsymbol{\Phi}_{\theta N}(\theta_0+2\pi,\theta_0)^T\mathbf{J}\boldsymbol{\Phi}_{\theta N}(\theta_0+2\pi,\theta_0) = (\mathbf{T}(\theta_0)^{-1}\boldsymbol{\Phi}_N(\theta_0 + 2\pi,\theta_0)\mathbf{T}(\theta_0))^T\mathbf{J}(\mathbf{T}(\theta_0)^{-1}\boldsymbol{\Phi}_N(\theta_0+2\pi,\theta_0)\mathbf{T}(\theta_0)) = \frac{1}{\dot{\theta}_0}\mathbf{T}(\theta_0)(\boldsymbol{\Phi}_N(\theta_0+2\pi,\theta_0)^T\mathbf{J}\boldsymbol{\Phi}_N(\theta_0+2\pi,\theta_0))\mathbf{T}(\theta_0) = \mathbf{J} \tag{88}$$

For $\mathbf{M}(n,\theta_0)$ to be symplectic, from Eq. (80), it must satisfy

$$[\mathbf{1}+\varepsilon\mathbf{M}_1(n,\theta_0)+\varepsilon^2\mathbf{M}_2(n,\theta_0)+\cdots]^T\boldsymbol{\Phi}_{\theta N}^T\mathbf{J}\boldsymbol{\Phi}_{\theta N}[\mathbf{1}+\varepsilon\mathbf{M}_1(n,\theta_0) + \varepsilon^2\mathbf{M}_2(n,\theta_0)+\cdots] = \mathbf{J} \tag{89}$$

By equating the same-order terms of ε, we obtain, for first order,

$$\mathbf{M}_1(n,\theta_0)^T\mathbf{J} + \mathbf{J}\mathbf{M}_1(n,\theta_0) = \mathbf{0} \tag{90}$$

and for second order,

$$\mathbf{M}_2(n,\theta_0)^T\mathbf{J} + \mathbf{J}\mathbf{M}_2(n,\theta_0) + \mathbf{M}_1(n,\theta_0)^T\mathbf{J}\mathbf{M}_1(n,\theta_0) = \mathbf{0} \tag{91}$$

Equation (90) provides the first-order symplectic condition. To satisfy it at any revolution number, all the parameter matrices $\mathbf{M}_{pm}$, $\mathbf{M}_{cm}$, and $\mathbf{M}_{sm}$ in Eq. (61) must satisfy Eq. (90) individually. If $\mathbf{M}_1(n,\theta_0)$ is divided into four submatrices as

$$\mathbf{M}_1(n,\theta_0) = \begin{bmatrix}\mathbf{M}_{1(1,1)} & \mathbf{M}_{1(1,2)}\\ \mathbf{M}_{1(2,1)} & \mathbf{M}_{1(2,2)}\end{bmatrix} \tag{92}$$

then Eq. (86) is equivalent to

$$\mathbf{M}_{1(1,1)} = -\mathbf{M}_{1(2,2)}^T, \qquad \mathbf{M}_{1(1,2)} = \mathbf{M}_{1(1,2)}^T, \qquad \mathbf{M}_{1(2,1)} = \mathbf{M}_{1(2,1)}^T \tag{93}$$

The condition Eq. (93) implies that there are only 15 independent elements in 6×6 matrix $\mathbf{M}_1(n,\theta_0)$. Therefore, by taking into account the first-order symplectic structure, the total number of parameters to be determined is reduced from the original $36q_A$ to $15q_A$, where q_A is defined in Eq. (67). The same thing is true for $\mathbf{N}_{ck}$ and $\mathbf{N}_{sk}$, which means that the parameters for the approximate state transition matrix with an interpolation between one orbit is reduced from $36q$ to $15q$.

C. Modifier Matrix to Satisfy Second-Order Symplecticity

It will be shown later that the first-order symplectic condition does not always provide sufficient accuracy in terms of symplecticity. The second-order symplectic condition Eq. (91) can be used to improve this symplecticity error.

For a given $\mathbf{M}_1(n,\theta_0)$ (by curve-fitting), if $\mathbf{M}_2(n,\theta_0)$ is found such that they satisfy Eq. (91), the resulting approximate state transition matrix would be second-order symplectic. Because $\mathbf{M}_2(n,\theta_0)$ in Eq. (87) is a second-order term, the effect of the addition of $\mathbf{M}_2(n,\theta_0)$ is, at most, of second order. Therefore, such an $\mathbf{M}_2(n,\theta_0)$ is expected to provide second-order accuracy on symplecticity without affecting the first-order accuracy of the approximate state transition matrix obtained by curve-fitting.

To solve Eq. (91), let the equation be rewritten in the following vectorized form:

$$\begin{aligned}&\text{vec}\{\mathbf{M}_2(n,\theta_0)^T\mathbf{J}\} + \text{vec}\{\mathbf{J}\mathbf{M}_2(n,\theta_0)\}\\&\quad = -\text{vec}\{\mathbf{M}_1(n,\theta_0)^T\mathbf{J}\mathbf{M}_1(n,\theta_0)\}\\&\quad \Rightarrow \mathbf{H}\mathbf{a} = -\mathbf{b},\\&\mathbf{H} \triangleq [-(\mathbf{J}\otimes\mathbf{1}_{6\times6})\mathbf{E} + (\mathbf{1}_{6\times6}\otimes\mathbf{J})], \qquad \mathbf{a} \triangleq \text{vec}\{\mathbf{M}_2(n,\theta_0)\},\\&\mathbf{b} \triangleq \text{vec}\{\mathbf{M}_1(n,\theta_0)^T\mathbf{J}\mathbf{M}_1(n,\theta_0)\}\end{aligned} \tag{94}$$

where $\otimes$ represents the Kronecker product and $\mathbf{E}$ is a 36×36 square matrix that satisfies $\text{vec}\{\mathbf{M}\} = \mathbf{E}\cdot\text{vec}\{\mathbf{M}^T\}$. $\mathbf{H}$, $\mathbf{a}$, and $\mathbf{b}$ are 36×36, 36×1, and 36×1 matrix and vectors, respectively. Note that $\mathbf{H}$ is a constant matrix with $\text{rank}\mathbf{H} = 15$. The independent elements of $\mathbf{b}$ are also 15. Thus, Eq. (94) is solvable for $\mathbf{a}$ but is an underdetermined condition. Hence, denoting $\mathbf{K}$ as a 15×36 matrix that extracts 15 independent elements from $\mathbf{b}$, one of the solutions can be obtained by minimizing the following objective function:

$$J = \tfrac{1}{2}\mathbf{a}^T\mathbf{a} + \boldsymbol{\lambda}^T(\mathbf{K}\mathbf{H}\mathbf{a} - \mathbf{K}\mathbf{b}) \tag{95}$$

where $\boldsymbol{\lambda}$ is a conjugate vector. Consequently, $\mathbf{M}_2(n,\theta_0)$ can be obtained by the following one-step procedure:

$$\begin{aligned}\mathbf{M}_2(n,\theta_0) = \text{vec}^{-1}\{&(\mathbf{K}\mathbf{H})^T[(\mathbf{K}\mathbf{H})(\mathbf{K}\mathbf{H})^T]^{-1}\mathbf{K}\\&\cdot\text{vec}\{\mathbf{M}_1(n,\theta_0)^T\mathbf{J}\mathbf{M}_1(n,\theta_0)\}\}\end{aligned} \tag{96}$$

where vec^{-1} is an inverse operation of Eq. (68). Note that $(\mathbf{K}\mathbf{H})^T[(\mathbf{K}\mathbf{H})(\mathbf{K}\mathbf{H})^T]^{-1}\mathbf{K}$ is a constant matrix. Therefore, for onboard applications, for example, this matrix can be preset in onboard software.

D. Numerical Validations of the Symplectic Approximate State Transition Matrix

Figure 9 shows the fitting quality, determinant, and symplecticity error for the cases p2s2m4, p2s2m4-symp1, and p2s2m4-symp2. Case p2s2m4 is the approximation without imposing the symplectic constraints. Case p2s2m4-symp1 is the first-order symplectic constrained, and p2s2m4-symp2 is the second-order symplectic constrained. The numbers of matrices and parameters for these cases are shown in Table 1.

Figure 9 indicates that the fitting quality is in the same error range regardless of the addition of constraints. Cases p2s2m4-symp1 and p2s2m4-symp2 are almost overlapped, which means that the second-order symplecticity modifier Eq. (96) does not affect the fitting quality.

The determinant error and symplecticity are evaluated by

$$\begin{aligned}\text{determinant error} &= |\det\boldsymbol{\Phi}_P - 1|\\ \text{symplecticity} &= \|\boldsymbol{\Phi}_P^T\mathbf{J}\boldsymbol{\Phi}_P - \mathbf{J}\|\end{aligned} \tag{97}$$

Case p2s2m4-symp1 does not improve the determinant and symplectic properties as compared with p2s2m4. This is because the source matrix data are generated by the numerical-symplectic state transition matrix [20], which is very precise in terms of the symplecticity, and p2s2m4 already has more than first-order accuracy in symplecticity. Therefore, by adding constraints in p2s2m4-symp1, the adaptability for fitting decreases and, as a consequence, the symplecticity is not improved, but rather slightly deteriorated.

This situation is improved by p2s2m4-symp2, which drastically improves the determinant error and the symplecticity, as is expected from the discussions in the previous subsection. Thus, for the second-order symplectic approximate state transition matrix, it can be said that the fundamental mathematical structure of a Hamiltonian system is preserved. It also leads to a justification of the use of nice properties of symplectic matrices, such as Eq. (83), for practical implementation of the approximate state transition matrix to actual missions.

VI. Conclusions

An approximation method for state transition matrices for orbits around a primary body subject to arbitrary perturbation forces was derived. The generalized averaging method for linear differential equations with almost-periodic coefficients was employed to isolate high- and low-frequency spectra in perturbation terms, and it constructed a functional form of the approximate state transition matrix composed only of elementary analytic functions. The resulting state transition matrix is expressed with a small number of constant parameter matrices and osculating orbit parameters at the initial epoch, and is valid for tens of orbital revolutions without updating the parameters. In typical relative orbit calculations, an accuracy level of 0.1–1% of relative distance between spacecraft is achieved for arbitrary-eccentricity orbits with a semimajor axis ranging from LEO up to around 10 Earth radii when applied to Earth orbits. It is also shown that the symplectic property of state transition matrices can be incorporated into the method, which not only improves the geometrical preciseness of the derived state transition matrix, but also reduces the number of parameters required for approximations. Because of the simplicity and good approximation accuracy of this method, the approximated representations proposed in this paper can be implemented onboard spacecraft or used for ground-based analyses when fast and iterative computations of accurate state transition matrices are necessary.

Appendix A: State Transition Matrix for Two-Body Orbital Dynamics

This section provides the concrete expression of $\boldsymbol{\Phi}_{\theta N}$, the state transition matrix of two-body (Keplerian) orbit observed in inertial coordinates, which corresponds to the solution for Eq. (7) when $\varepsilon = 0$. The derivation here is based on [8].

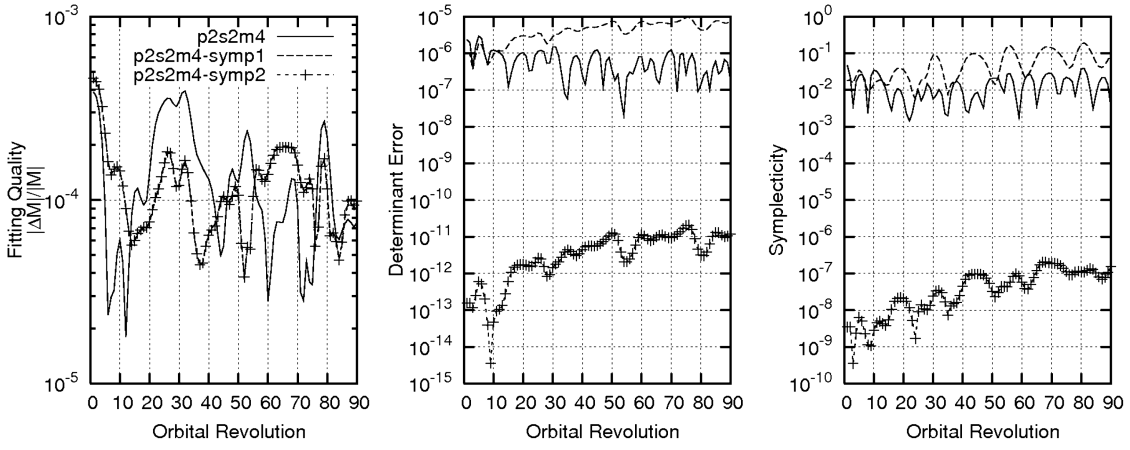

Fig. 9 Performance of symplecticity-constrained approximation.

The derivation begins with obtaining a state transition matrix expressed in a rotational coordinate frame. For this purpose, let us introduce a coordinate transformation matrix $\mathbf{Q}$ such that the inertial coordinates is transformed to the rotating coordinates with the x axis pointing toward the radial direction, the z axis perpendicular to the orbital plane, and the y axis completes the right-hand system. Hence, this transformation can be expressed as

$$\delta\mathbf{x}^R = \mathbf{Q}\delta\mathbf{x} = \begin{bmatrix} \mathbf{P} & \mathbf{0} \\ \mathbf{P}' & \mathbf{P} \end{bmatrix} \begin{bmatrix} \delta\mathbf{r} \\ \delta\dot{\mathbf{r}} \end{bmatrix}, \qquad \mathbf{P} = \begin{bmatrix} \cos\theta & \sin\theta & 0 \\ -\sin\theta & \cos\theta & 0 \\ 0 & 0 & 1 \end{bmatrix} \tag{A1}$$

where $\delta\mathbf{x}$ and $\delta\mathbf{x}^R$ are state vectors expressed in the inertial and rotating coordinates, respectively, and θ is the true anomaly. Using this notation, the state transition matrix expressed in the rotational coordinates is related with one expressed in the inertial coordinates as

$$\mathbf{\Phi}_{\theta N}(\theta_2, \theta_1) = \mathbf{Q}(\theta_2)^{-1}\mathbf{\Phi}^R_{\theta N}(\theta_2, \theta_1)\mathbf{Q}(\theta_1) \tag{A2}$$

The 6×6 matrix $\mathbf{\Phi}^R_{\theta N}$ is obtained as follows:

$$\mathbf{\Phi}^R_{\theta N}(\theta_2, \theta_1) = \Gamma(\theta_2)\Gamma(\theta_1)^{-1} \tag{A3}$$

where

$$\Gamma(\theta) = \{p_{ij}(\theta)\}, \qquad i, j = 1, 2, \ldots, 6 \tag{A4}$$

$$\begin{gathered} p_{11} = e\sin\theta, \qquad p_{12} = 2e^2H(\theta)\sin\theta - \frac{e\cos\theta}{(1+e\cos\theta)^2} \\ p_{13} = -\cos\theta, \qquad p_{21} = 1 + e\cos\theta \\ p_{22} = 2eH(\theta) + 2e^2H(\theta)\cos\theta, \qquad p_{23} = \sin\theta + \frac{\sin\theta}{1+e\cos\theta} \\ p_{24} = \frac{1}{1+e\cos\theta}, \qquad p_{35} = \frac{\sin\theta}{1+e\cos\theta} \\ p_{36} = \frac{\cos\theta}{1+e\cos\theta}, \qquad p_{41} = p'_{11}, \qquad p_{42} = p'_{12} \\ p_{43} = p'_{13}, \qquad p_{51} = p'_{21}, \qquad p_{52} = p'_{22}, \qquad p_{53} = p'_{23} \\ p_{54} = p'_{24}, \qquad p_{65} = p'_{35}, \qquad p_{66} = p'_{36}, \quad \text{otherwise } p_{ij} = 0 \end{gathered} \tag{A5}$$

and

$$\begin{gathered} H(\theta) = -(1+e^2)^{3/2}\left[\frac{3eE}{2} - (1+e^2)\sin E + \frac{e}{2}\sin E\cos E\right] \\ H'(\theta) = \frac{\cos\theta}{(1+e\cos\theta)^3} \end{gathered} \tag{A6}$$

where E is the eccentric anomaly associated with θ. Note that this derivation is valid for $e \neq 0$. For a circular-orbit case, one can simply use the solution for Hill's equations, and the similar relations can be obtained. By using Eqs. (A1–A6), we can concretely calculate each element of the state transition matrix using only elementary functions.

Because the system equation (7) (with $\varepsilon = 0$) is a differential equation with periodic coefficients, we know from Floquet's theorem that there is a monodromy matrix $\mathbf{M}_N$ (constant matrix) that satisfies

$$\mathbf{\Phi}_{\theta N}(\theta + 2\pi, 0) = \mathbf{\Phi}_{\theta N}(\theta, 0)\mathbf{M}_N \tag{A7}$$

Hence, the state transition matrix over each orbital period is derived as

$$\mathbf{\Phi}_{\theta N}(\theta + 2\pi, \theta) = \mathbf{\Phi}_{\theta N}(\theta, 0)\mathbf{M}_N\mathbf{\Phi}_{\theta N}(\theta, 0)^{-1} \tag{A8}$$

Using the derivation of the state transition matrix in Eqs. (A1–A6) and (A8), the monodromy matrix is concretely calculated as follows:

$$\mathbf{M}_N = \mathbf{\Phi}_{\theta N}(2\pi, 0) = \mathbf{1}_{6\times 6} + \mathbf{W}_0 \tag{A9}$$

where $\mathbf{W}_0$ is a constant matrix given as

$$\mathbf{W}_0 = \mathbf{Q}^{-1}\begin{bmatrix} 0 & 0 & 0 & 0 & 0 & 0 \\ -w_{21} & 0 & 0 & 0 & -w_{25} & 0 \\ 0 & 0 & 0 & 0 & 0 & 0 \\ -w_{41} & 0 & 0 & 0 & -w_{45} & 0 \\ 0 & 0 & 0 & 0 & 0 & 0 \\ 0 & 0 & 0 & 0 & 0 & 0 \end{bmatrix}\mathbf{Q} \tag{A10}$$

where we abbreviate $\mathbf{Q}(0) = \mathbf{Q}(2\pi) = \mathbf{Q}$, and

$$\begin{aligned} w_{21} &= \frac{6(1+e)(2+e)\pi}{(-1+e)^2\sqrt{1-e^2}}, & w_{25} &= \frac{6(1+e)^2\pi}{(-1+e)^2\sqrt{1-e^2}} \\ w_{41} &= \frac{6e(2+e)\pi}{(-1+e)^2\sqrt{1-e^2}}, & w_{45} &= \frac{6e(1+e)\pi}{(-1+e)^2\sqrt{1-e^2}} \end{aligned} \tag{A11}$$

By noting the equality

$$\mathbf{W}_0^2 = \mathbf{0} \tag{A12}$$

the following useful relations are derived:

$$\mathbf{M}_N = e^{\mathbf{W}_0} \tag{A13}$$

$$\mathbf{M}_N^{-1} = \mathbf{1}_{6\times 6} - \mathbf{W}_0 \tag{A14}$$

$$\mathbf{\Phi}_{\theta N}(2n\pi, 0) = \mathbf{M}_N^n = e^{n\mathbf{W}_0} = \mathbf{1}_{6\times 6} + n\mathbf{W}_0 \tag{A15}$$

Equation (A15) provides the secular term of $\mathbf{\Phi}_{\theta N}$, and the rest of the terms of $\mathbf{\Phi}_{\theta N}$ are to be all 2π-periodic. Thus, Eq. (10) is proved. From Eqs. (A9) and (A15), we also get

$$\mathbf{\Phi}_{\theta N}(\theta_0 + 2n\pi, \theta_0) = \mathbf{1}_{6\times 6} + n\mathbf{W}(\theta_0) \tag{A16}$$

where $\mathbf{W}(\theta_0) = \mathbf{\Phi}_{\theta N}(\theta_0, 0)\mathbf{W}_0\mathbf{\Phi}_{\theta N}(\theta_0, 0)^{-1}$.

To transform to a time-domain expression, the transformation matrix $\mathbf{T}$ given in Eq. (6) is used, and thus,

$$\mathbf{\Phi}_N(t_2, t_1) = \mathbf{T}(t_2)^{-1}\mathbf{\Phi}_{\theta N}(\theta(t_2), \theta(t_1))\mathbf{T}(t_1) \tag{A17}$$

Appendix B: Generalized Averaging Method

The general procedure of the generalized averaging method for linear differential equations with almost-periodic coefficients. This procedure is based on [1].

The basic system to be dealt with is the following linear differential equation:

$$\dot{\mathbf{x}} = \mathbf{A}(t)\mathbf{x} \tag{B1}$$

where $\mathbf{A}(t)$ takes the specific form

$$\mathbf{A}(t) = \sum_n (\mathbf{A}_n\cos\omega_n t + \mathbf{B}_n\sin\omega_n t) \tag{B2}$$

Equation (B2) is one of the general representations of an *almost-periodic function*. The problem to be solved here is to obtain the averaged solution for Eq. (B1) by taking into account only the effect of the lower-frequency part of Eq. (B2).

If the averaging and integration operators defined in Eq. (20) are applied to Eq. (B2), we obtain

$$\left.\begin{aligned} L_{\omega_c}[\mathbf{A}(t)] &= \sum_{0\le\omega_n<\omega_c} (\mathbf{A}_n\cos\omega_n t + \mathbf{B}_n\sin\omega_n t) \\ H_{\omega_c}[\mathbf{A}(t)] &= \sum_{\omega_c\le\omega_n} \omega_n^{-1}(\mathbf{A}_n\cos\omega_n t + \mathbf{B}_n\sin\omega_n t) \end{aligned}\right\} \tag{B3}$$

$$\frac{\mathrm{d}}{\mathrm{d}t}H_{\omega_c}[\mathbf{A}(t)] = \mathbf{A}(t) - L_{\omega_c}[\mathbf{A}(t)] \tag{B4}$$

Now let us transform $\mathbf{x}$ to a new vector $\mathbf{y}$ by

$$\mathbf{y} = (\mathbf{1} + \mathbf{V}(t))\mathbf{x} \tag{B5}$$

where $\mathbf{1}$ is the identity matrix and $\mathbf{V}(t)$ is to be determined at this point. Then assume that the transformed differential equation for $\mathbf{y}$ is of the form

$$\dot{\mathbf{y}} = \mathbf{L}(t)\mathbf{y} \tag{B6}$$

where $\mathbf{L}(t)$ is also to be determined. Substituting Eqs. (B5) and (B6) into Eq. (B1), we obtain the following equation for $\mathbf{V}(t)$:

$$\dot{\mathbf{V}}(t) = \mathbf{U}(t) - \mathbf{L}(t) \tag{B7}$$

where

$$\mathbf{U}(t) = \mathbf{A}(t) + \mathbf{A}(t)\mathbf{V}(t) - \mathbf{V}(t)\mathbf{L}(t) \tag{B8}$$

We desire to choose $\mathbf{L}(t)$ in such a way that the solution to Eq. (B7) for $\mathbf{V}(t)$ is bounded for all t regardless of the form of $\mathbf{U}(t)$. By assuming that $\mathbf{U}(t)$ is of the same form as $\mathbf{A}(t)$ [i.e., of the form Eq. (B2)], this leads to

$$\mathbf{L}(t) = L_{\omega_c}[\mathbf{U}(t)] \tag{B9}$$

where ω_c is a cutoff frequency to appropriately extract the region having low frequency. The solution for $\mathbf{V}(t)$ then becomes

$$\mathbf{V}(t) = H_{\omega_c}[\mathbf{U}(t)] + \mathbf{V}_0 \tag{B10}$$

where $\mathbf{V}_0$ is an arbitrary constant matrix and it can be treated as zero in the current development.

For $\mathbf{V}(t)$ and $\mathbf{L}(t)$ to be consistent, the condition for $\mathbf{U}(t)$ is derived from Eqs. (B7–B10) as

$$\mathbf{U}(t) = \mathbf{A}(t) + \mathbf{A}(t)H_{\omega_c}[\mathbf{U}(t)] - H_{\omega_c}[\mathbf{U}(t)]L_{\omega_c}[\mathbf{U}(t)] \tag{B11}$$

If $\mathbf{U}(t)$ is found such that it satisfies Eq. (B11), the governing equation for $\mathbf{y}$, which is the averaged behavior of $\mathbf{x}$, can be found through obtaining $\mathbf{L}(t)$ by Eq. (B9) and substituting it into Eq. (B6). Therefore, $\mathbf{U}(t)$ is called the generating function of the transformation equation (B5).

There are several ways to solve Eq. (B11). If one uses successive approximation, the sufficient condition to guarantee the existence of solutions is given by

$$\|\mathbf{A}(t)\| < (3 - 2\sqrt{2})\omega_c \approx 0.172\omega_c \tag{B12}$$

The proof for this is given in [26]. As is mentioned in [1,26], Eq. (B12) is a rather conservative sufficient condition, and there may exist a solution even when Eq. (B12) is violated.

References

[1] Coakley, T. J., "A Generalized Averaging Method for Linear Differential Equations with Almost Periodic Coefficients," NASA TN D-5167, 1969.

[2] Hill, G. W., "Researches in the Lunar Trajectory," *American Journal of Mathematics*, Vol. 1, 1878, pp. 5–26. doi:10.2307/2369430

[3] Clohessy, W. H., and Wiltshire, R. S., "Terminal Guidance System for Satellite Rendezvous," *Journal of the Astronautical Sciences*, Vol. 27, No. 9, 1960, pp. 653–678.

[4] Lawden, D. F., *Optimal Trajectories for Space Navigation*, Buttherworths, London, 1963.

[5] Carter, T. E., and Humi, M., "Fuel-Optimal Rendezvous Near a Point in General Keplerian Orbit," *Journal of Guidance, Control, and Dynamics*, Vol. 10, No. 6, 1987, pp. 567–573. doi:10.2514/3.20257

[6] Carter, T. E., "New Form For the Optimal Rendezvous Equations Near a Keplerian Orbit," *Journal of Guidance, Control, and Dynamics*, Vol. 13, No. 1, 1990, pp. 183–186. doi:10.2514/3.20533

[7] Ross, M., "Linearized Dynamic Equations for Spacecraft Subject to J2 Perturbations," *Journal of Guidance, Control, and Dynamics*, Vol. 26, No. 4, 2003, pp. 657–659. doi:10.2514/2.5095

[8] Inalhan, G., Tillerson, M., and How, J., "Relative Dynamics and Control of Spacecraft Formations in Eccentric Orbits," *Journal of Guidance, Control, and Dynamics*, Vol. 25, No. 1, 2002, pp. 48–59. doi:10.2514/2.4874

[9] Hamel, J. H., and Lafontaine, J., "Linearized Dynamics of Formation Flying Spacecraft on a J2-Perturbed Elliptical Orbit," *Journal of Guidance, Control, and Dynamics*, Vol. 30, No. 6, 2007, pp. 1649–1658. doi:10.2514/1.29438

[10] Gim, D. W., and Alfriend, K. T., "The State Transition Matrix for Relative Motion of Formation Flying Satellites," AAS Space Flight Mechanics Meeting, American Astronautical Society, Paper 02-186, San Antonio, TX, 2002.

[11] Gim, D. W., and Alfriend, K. T., "State Transition Matrix of Relative Motion for the Perturbed Non-Circular Reference Orbit," *Journal of Guidance, Control, and Dynamics*, Vol. 26, No. 6, 2003, pp. 956–971. doi:10.2514/2.6924

[12] Alfriend, K. T., Yan, H., and Vadali, S. R., "Nonlinear Consideration in Satellite Formation Flying," AIAA/AAS Astrodynamics Specialist Conference and Exhibit, AIAA Paper 2002-4741, 2002.

[13] Vaddi, S. S., Vadali, S. R., and Alfriend, K. T., "Formation Flying: Accommodating Nonlinearity and Eccentricity Perturbations," *Journal of Guidance, Control, and Dynamics*, Vol. 26, No. 2, 2003, pp. 214–223. doi:10.2514/2.5054

[14] Melton, R. G., "Time-Explicit Representation of Relative Motion Between Elliptic Orbits," *Journal of Guidance, Control, and Dynamics*, Vol. 23, No. 4, 2000, pp. 604–610. doi:10.2514/2.4605

[15] Park, R. S., and Scheeres, D. J., "Nonlinear Mapping of Gaussian Statistics: Theory and Applications to Spacecraft Trajectory Design," *Journal of Guidance, Control, and Dynamics*, Vol. 29, No. 6, 2006, pp. 1367–1375. doi:10.2514/1.20177

[16] Schaub, H., "Relative Orbit Geometry Through Classical Orbit Element Differences," *Journal of Guidance, Control, and Dynamics*, Vol. 27, No. 5, 2004, pp. 839–848. doi:10.2514/1.12595

[17] Halsall, M., and Palmer, P. L., "An Analytic Relative Orbit Model Incorporating J3," AIAA/AAS Astrodynamics Specialist Conference and Exhibit, AIAA Paper 2006-6761, Keystone, CO, 2006.

[18] Palmer, P. L., and Imre, E., "Relative Motion between Satellites on Neighboring Keplerian Orbits," *Journal of Guidance, Control, and Dynamics*, Vol. 30, No. 2, 2007, pp. 521–528. doi:10.2514/1.24804

[19] Imre, E., and Palmer, P. L., "High-Precision, Symplectic Numerical, Relative Orbit Propagation," *Journal of Guidance, Control, and Dynamics*, Vol. 30, No. 4, 2007, pp. 965–973. doi:10.2514/1.26846

[20] Tsuda, Y., and Scheeres, D. J., "Computation and Applications of an Orbital Dynamics Symplectic State Transition Matrix," 19th AAS/AIAA Space Flight Mechanics Meeting, American Astronautical Society, Paper 09-158, Savannah, GA, 2009.

[21] Xiang, W., and Jørgensen, J. L., "Formation Flying: A Subject Being Fast Unfolding in Space," *5th IAA Symposium on Small Satellites for Earth Observation*, International Academy of Astronautics Paper B5-0309P, Berlin, Germany, 2005.

[22] Sengupta, P., Vadali, S. R., and Alfriend, K. T., "Averaged Relative Motion and Applications to Formation Flying Near Perturbed Orbits," *Journal of Guidance, Control, and Dynamics*, Vol. 31, No. 2, 2008, pp. 258–272. doi:10.2514/1.30620

[23] Hsiao, F. Y., and Scheeres, D. J., "Fundamental Constraints on Uncertainty Evolution in Hamiltonian Systems," *IEEE Transactions on Automatic Control*, Vol. 52, No. 4, 2007, pp. 686–691. doi:10.1109/TAC.2007.894531

[24] Scheeres, D. J., Hsiao, F. Y., Park, R. S., Villac, B. F., and Maruskin, J. M., "Fundamental Limits on Spacecraft Orbit Uncertainty and Distribution Propagation,", *Journal of the Astronautical Sciences*, Vol. 54, 2006, pp. 505–523.

[25] Scheeres, D. J., Han, D., and Hou, Y., "Influence of Unstable Manifolds on Orbit Uncertainty," *Journal of Guidance, Control, and Dynamics*, Vol. 24, No. 3, 2001, pp. 573–585. doi:10.2514/2.4749

[26] Woodcock, D. L., Elton, D., and Davies, R. J., "An Examination of an Iterative Procedure for Determining the Characteristic Exponents of Linear Differential Equations with Periodic Coefficients," Aeronautical Research Council, Current Papers, No. 1218, 1972.